Cryogenic Photogrammetry & Radiometry for the James Webb Space Telescope Microshutters

Victor J. Chambers*[a], Peter A. Morey[b], Barbara J. Zukowski[b], Alexander S. Kutyrev[c], Nicholas R. Collins[d], Nargess Memarsadeghi[a], Samuel H. Moseley[a], Leroy M. Sparr[a], Peter N. Blake[a], Microshutter Team
[a]NASA Goddard Space Flight Center, Greenbelt, MD, 20771.
[b]Ball Aerospace and Technologies Corp., Lanham, MD, 20706.
[c]CRESST UMd NASA's GSFC
[d]Wyle NASA's GSFC

ABSTRACT

The James Webb Space Telescope (JWST) relies on several innovations to complete its five year mission. One vital technology is *microshutters*, the programmable field selectors that enable the Near Infrared Spectrometer (NIRSpec) to perform multi-object spectroscopy. Mission success depends on acquiring spectra from large numbers of galaxies by positioning shutter slits over faint targets. Precise selection of faint targets requires field selectors that are both high in contrast and stable in position. We have developed test facilities to evaluate microshutter contrast and alignment stability at their 35K operating temperature. These facilities used a novel application of image registration algorithms to obtain non-contact, sub-micron measurements in cryogenic conditions. The cryogenic motion of the shutters was successfully characterized. Optical results also demonstrated that shutter contrast far exceeds the NIRSpec requirements. Our test program has concluded with the delivery of a flight-qualified field selection subsystem to the NIRSpec bench.

Keywords: JWST, NIRSpec, spectography, microshutters, photogrammetry, image registration, field selector, optical metrology

1. INTRODUCTION

NASA's Goddard Space Flight Center (GSFC) has delivered a two-dimensional microshutter array for the James Webb Space Telescope's Near Infrared Spectrometer (NIRSpec). NIRSpec's primary science goal is to observe the epoch of the initial formation of galaxies by measuring the spectra of at least 2500 galaxies. [1] Since faint, high redshift targets are sparse and require long exposures, an efficient multi-object spectrograph is required to meet JWST's science goals within its 5 year mission. [2, 3] The microshutter array is a fully programmable field of silicon nitride shutter cells (Figure 1). By functioning as an addressable mask, they enable NIRSpec to complete multi-object spectroscopy on up to 100 objects simultaneously. They are designed to operate at JWST's 35K cryogenic temperature and will provide spectra of selected objects at wavelengths in the 0.6-5 μm range. The shutters are positioned at the focal plane of the NIRSpec instrument where they are designed to be both *high contrast* and *stable* focal plane object selectors. [4]

Since JWST requires obtaining spectra of extremely faint objects, high shutter contrast is essential. Our contrast requirement is defined as the ratio between the flux through an open shutter to that through a closed shutter. This contrast ratio must be greater than 2,000 in order to avoid having target spectra be polluted with the light from other nearby or bright sources in the same field of view and to eliminate noise from the zodiacal light diffuse background. A shutter that does not meet this requirement is considered a "failed open" and must be identified so that faint, high Z objects are not measured in close proximity. [5] The first half of this paper outlines NASA's efforts to optically characterize the contrast of the NIRSpec's Microshutters, and to identify 'failed open' shutters for repair or exclusion.

* john.chambers@nasa.gov; phone 1 301 286-9944; fax 1 301 286-1704

Given that JWST is primarily focused on high redshift, long wavelength targets, many sources will be diffraction limited through each shutter slit (overfilled). Sources clipped by shutter borders are particularly susceptible to intensity shifts. In particular, slight shutter misalignments would create overt spectro-photometric errors. Any errors caused by lateral shutter instability would effectively shift the measured spectra and produce wavelength and velocity errors for the source. In addition, instability in shutter focus would manifest as an unsharpened image of the slit and a blurred point spread function. Sixteen microns is the total NIRSpec error budget for shutter motion over a target, of which only one micron is allocated to the Micro-Shutter Assembly (MSA). [6] Since the budget is tight, it is essential to ensure that the MSA is stable in six degrees of freedom at 35K. Alignment requirements for the microshutter arrays include accurately defining their cryogenic displacement, knowledge of their position at operating temperature and stability of their position across the operational temperature range. Efforts made to optically characterize the position of the shutter arrays are discussed in the second portion of this paper. A summary of JWST's general scientific objectives is provided by Gardner et al. [7]

2. DESIGN AND FUNCTION OF THE MICROSHUTTER ASSEMBLY

The MSA is comprised of four array quadrants of 365 by 171 shutters assembled onto a base plate via titanium flexures. The shutters are close-packed silicon nitride membranes measuring 100 x 200 x 0.5 microns. Each shutter blade is fabricated with a single torsion bar hinge on the side and light shields that surround its front. The shields greatly reduce light leakage through the arrays. Figure 1 shows magnified images of the closed shutters. The initial development of microshutters was managed by the University of Maryland before being transferred to the Detector Development Laboratory (DDL) at the Goddard Space Flight Center. [8] The DDL employed a combination of microlithography techniques to form the shutter structure including a unique Deep Reactive Ion Etch (DRIE) process to create the rear 'egg crate' support structure. [9] The DDL fabrication process includes coating each shutter blade with thin bands of CoFe. This ferrous material allows each shutter to be magnetically actuated, after which they are electrostatically addressed and held open. Selecting a dual electro-magnetic process alleviated the necessity for prohibitively high voltages to latch open shutter arrays. The MSA latching process works by scanning a magnet behind the array so that shutters are rotated downward until they are electrostatically held open by the structure walls. [10] Applying sufficient electrical bias via a cross-addressing method holds selected shutters open to form a desired pattern. Shutters not addressed with sufficient 'hold' voltage are returned to their released position by their spring-like torsion hinge. In the event that a shutter blade or light shield is damaged from use, the blade may not return to its 'released' position properly. Partially open or damaged shutters were identified as low contrast 'failed opens', so that they could be covered with aluminum plugs prior to MSA delivery.

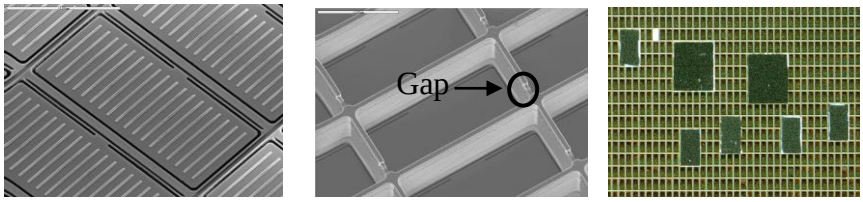

Figure 1. High magnification images of 100 × 200 micron shutters: left image shows front-side featuring torsion hinges on long edge and magnetic strips across breadth (light shields not pictured), middle image shows backside structure with electrical gaps labeled, right image shows aluminum plugs bonded to surface to cover failed-open shutters.

The MSA assembly shown in Figure 2 features four array quadrants mounted via titanium flexures onto a base plate with the shutter fields in the center. The 2 × 2 mosaic produces a total format of 342 × 730 shutters. However, the shutter fields are not mounted such that the quadrants contact each other. The quadrants are separated by 1mm in the dispersive (X) direction and by 7mm in the cross-dispersive (Y) direction. A titanium cruciform is installed directly behind the four quadrants, blocking light from passing through the gaps. This cruciform provides real-estate for several fixed slits and an Integral Field Unit (IFU) aperture. The center of both the four quadrants and the cruciform is the location of the MSA's Optical Reference Frame (ORF). During cool down, the quadrants move towards the ORF in a stable and predictable manner. Characterizing their positions on the assembly at the 35K operating temperature is essential for sustaining the quality of science produced by NIRSpec.

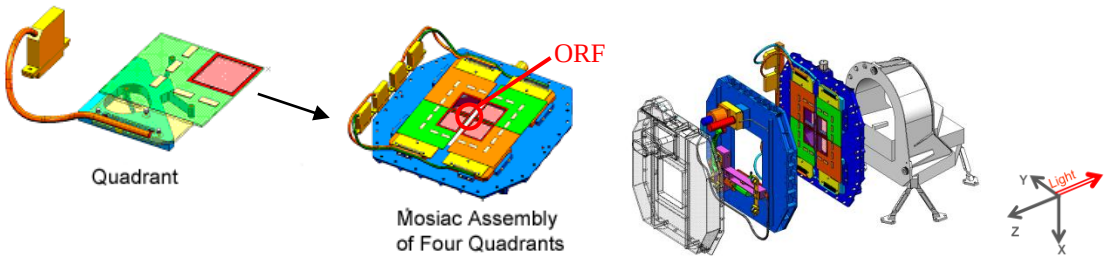

Figure 2. Schematics of a single quadrant, 4 quadrants mounted on the mosaic base plate and an exploded view of the MSA assembly. Shutter rows are oriented in the +Y, cross-dispersive direction and columns are oriented in the +X, dispersive direction (where shutter blades open along their column direction). The NIRSpec boresight and MSA Optical Reference Frame (ORF) are labeled on the base plate image.

3. QUALIFICATION OF MICROSHUTTER ARRAY QUADRANTS

3.1 Quadrant Evaluation: facility design and stray-light suppression

Three facilities have been developed to characterize array performance at their 35K operating temperature. Two of the three are identical systems created to carry out MS quadrant qualification and were designed for measurements of single quadrants only. The third is a larger system intended for characterization of the full MSA structure. Each of the three systems is designed to evaluate the electrical, mechanical and optical functionality of all 249,660 shutters *individually*. Our test systems were used to evaluate the optical performance of the microshutters at both visible (0.6 μm) and NIRSpec's IR bandpass (0.6-5μm). A schematic of the quadrant evaluation facilities is shown in Figure 3. A schematic of the MSA evaluation facility is shown in Section 4.

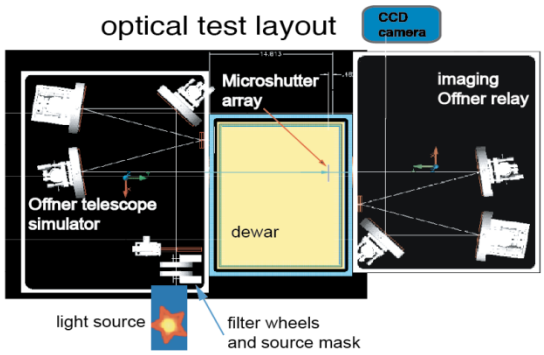

Figure 3. Design of the quadrant-level cryogenic metrology system with F/10 illumination. The central cryostat is bordered by a 'telescope simulator' (left) and imaging relay (right) that forms an unmagnified image of the array onto the camera sensor. Single quadrants are mounted in the dewar with requisite latching hardware to undergo electrical and optical metrology.

The quadrant-level evaluation facility is comprised of a central cryostat bordered by two identical 'Offner' imaging systems. [11] Each left-side 'telescope simulator' is designed to closely reproduce the NIRSpec F/12 telescope beam at the arrays. It features a filterable 633nm light source with an adjustable aperture, a primary mirror comprised of two 6-inch spherical mirrors and a smaller spherical 2-inch secondary mirror. The right-side optical relay forms an unmagnified image of the array onto the sensor of an Apogee U16M 16-bit camera. The camera features 4096 × 4096 nine-micron pixels, making the detector size slightly smaller than the quadrant shutter field. A small de-magnifying lens is mounted in front of the camera to allow full-quadrant imaging. The CCD was switched with a smaller InSb 256 × 256 Spitzer IRCAM detector for imaging sub-sections of the quadrant in the IR. The dewar interior is equipped with the requisite quadrant electronics as well as a mechanism for positioning and sweeping the latching magnet. Initial testing revealed faulty performance caused by stray light and ghost images. The ghost images were eliminated by tilting the dewar windows and adding AR coatings. Adding baffles further reduced stray light on 'healthy' shutters to the level of 10^{-5},

well lower than magnitudes capable of degrading measurements near our contrast requirement of 2,000. Scattered light caused by broken or otherwise 'failed open' shutters remained a concern until remedied by masking the failures at the source. Transparent masks printed with opaque spots were mounted at the conjugate plane of the array, just behind the light source. After aligning the 'source mask' such that spots covered each failed open shutter, scatter was reduced enough to avoid affecting the measured contrast of adjacent shutters.

After quadrant images were masked to eliminate scatter, a procedure was followed to acquire sufficient signal-to-noise-ratio for accurate contrast measurements. Due to typically high shutter contrast, the limiting factor for measurement accuracy was detecting sufficient signal over background noise through released (closed) shutters. Acquiring several long exposures of the released shutters was necessary for adequate signal measurement. Images taken of the array included ten released (array closed) images with 100-second exposure times, ten latched (array open) images with two-second exposure times, a matching number of background measurements (source off) and measurement of the field uniformity. The open and closed images were then stacked with their backgrounds subtracted using a customized Interactive Data Language® (IDL) software routine. Using additional IDL routines, images were rotated, normalized to the flat field, and de-warped to compensate for optical distortion effects. A software mask was then used to remove the source-mask-blocked shutters from contrast results. Custom analysis software then applied the open/closed contrast ratio shown in Formula 1 averaged over each individual microshutter. Finally, the software presents results in graphic and tabular formats of the measured contrast value of every shutter as well as average array contrast and number of additional 'failed opens' detected. Our measurement and analysis process was employed at least three times per array quadrant in order to identify and plug low contrast (<2000) shutters. Extended life tests and contrast measurements ensured four robust quadrants were delivered to the Engineering Test Unit (ETU) MSA as well as the flight MSA.

$$Contrast = \frac{20\,\text{sec.latched} - 20\,\text{sec.background}}{1000\,\text{sec.released} - 1000\,\text{sec.background}} \quad (1)$$

3.2 Quadrant Evaluation: procedure and contrast results

Images and contrast maps from quadrant-level metrology performed on a flight-designated quadrant are shown in Figure 4. The latched and released images show the extent that failed opens have been patched with small aluminum coated Silicon 'plugs'. Approximately four leaking areas remain visible in the released image. Open shutters and 'failed opens' appear bright as all images were taken in transmitted light. Black 'source mask' spots are clearly discernible on the visible and IR contrast maps. They are aligned over failed shutters such that leaks do not degrade the measured contrast of neighboring shutters. During qualification, the average 633nm contrast for flight quadrant number four was 25,378 ± 10% with 144 total failed opens. Due to the size and resolution of the IR detector, a 3 × 3 mosaic was acquired. Thorough examination of both magnified IR and visible images established that shutters transmit light in the IR via a different path than that of visible light. Whereas visible light leakage is dominated by the degree that light passes around slightly bowed shutter blades, IR leakage is dominated by support structure transmission. Two micron gaps required in the 'egg crate' structure to avoid electrical shorts allow transmission and scattering through the silicon structure such that the structure 'glows' uniformly when illuminated in the IR (Figures 7 & 8) [12]. As a consequence, IR contrast is less dependent on measurement position and leakage is dependent on wavelength and scattering angle through the structure. Earlier tests of quadrants measured in the J (1.2 μm), H (1.6 μm) and K (2.2 μm) bands showed contrast consistently lowest in the H-band instead of at the 1.1 μm silicon transmission band. Based on these observations, IR contrast measurements were limited to the 1.6 μm H band where the modal contrast of quadrant four was 7,600 ± 10% with one additional failure. At the time that the flight MSA was delivered, the quadrant qualification program had evaluated the performance of 22 quadrants. The eight best performing quadrants were integrated onto the ETU and Flight MSA structures.

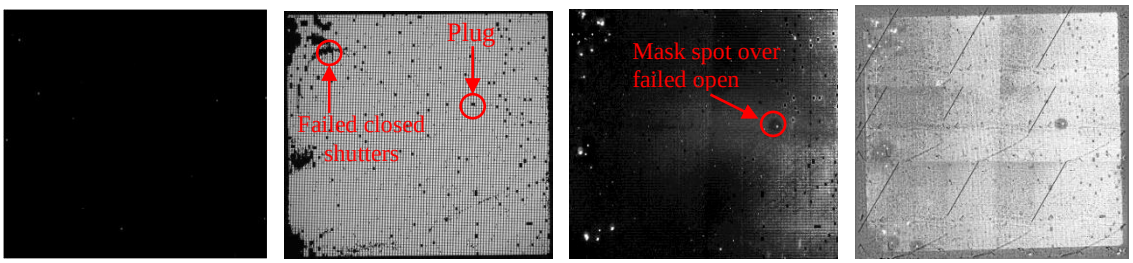

Figure 4. Images and contrast maps of Flight quadrant Q4-55-116 during quadrant-level metrology (post first round of plugging): a) image of all shutters released, b) image of all shutters latched open, c) visible contrast map where each pixel represents a single shutter's contrast value in grayscale, d) contrast map in IR (1.6 μm). Images of the 171 × 365 shutter array are acquired in transmitted light such that open shutters appear bright. Quadrant plugs, leaks and mask spots are labeled.

4. MSA OPTICAL METROLOGY: CONTRAST EVALUATION

4.1 Design of MSA Evaluation Facility

Following a successful qualification program, four quadrants were mounted to both the ETU and flight MSA structures as shown in Figure 2. Space requirements for the full field of shutters on the MSA hardware necessitated a larger MSA contrast evaluation facility. In addition to evaluating the contrast and functionality of the MSA shutters, it was necessary for the facility to verify their alignment requirements. The MSA-level facility shown in Figure 5 was designed to be a high-accuracy, cryogenic, non-contact photogrammetry test bed. It is unique in its capability to characterize both sub-micron cryogenic motion as well as the contrast of single-shutter array elements during their operation at 35K. Like the quadrant evaluation facilities, it is capable of measuring the contrast ratio of each individual shutter on the MSA. It does so one quadrant at a time by positioning its telescope simulator and imaging system in tandem with three-axis stages.

Like the quadrant facilities, the MSA facility consists of a central cryostat bordered by two imaging systems. Its cryogenic chamber is capable of achieving temperatures down to 15K while keeping a high vacuum ($<10^{-6}$ Torr). It has a larger set of seven inch optical ports on opposite sides of the chamber. The right side imagining system is identical to that of the single quadrant test facilities; however, the telescope simulator design is altered to allow for the increased distance between the dewar window and the illuminated side of the shutters. The updated design includes a diffused 632 nm LED array, a rotational stage to mount a 'source mask' and a two lens imaging system. The LEDs and diffuser are positioned to create a uniform beam and are controlled through system software. Like the single quadrant facilities, both front and rear imaging systems simulate the NIRSpec F/12 beam with near one-to-one magnification. Both the rear illumination system and the Offner optics are mounted on 3-axis translational stages attached to a single rigid structure. The stages are controlled through automated software and are used to position the Offner and the rear illumination to within 5 microns.

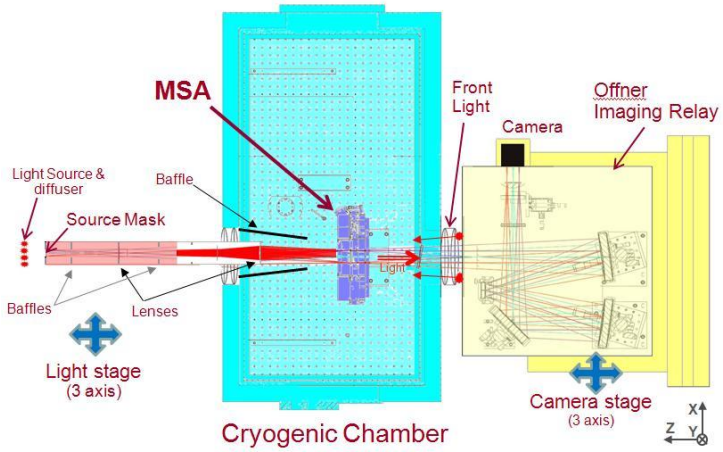

Figure 5. Schematic of the MSA evaluation facility showing telescope simulator on the left, the MSS dewar in center and the imaging optics with the CCD camera on the right. Both front and rear optical systems are mounted on fully-automated 3-axis stages. Front-side LEDS are required for quadrant alignment images.

4.2 Test system calibration

The performance of both the quadrant and MSA test facilities were carefully evaluated with several calibration methods. Statistical error was determined to be negligible by demonstrating a high degree of measurement and analysis repeatability. A strong camera SNR of 300 also implied negligible read noise. Systematic error from camera linearity was also examined by plotting average counts against varied exposure time (Figure 6). The data showed camera performance was clearly linear across our relevant exposure times. The limiting error source for all systems was systematic in nature. This was the capacity of stray light to limit accuracy when measuring contrast. Stray light calibration was done to ensure that stray light and scatter did not degrade contrast measurement capability below the 2K requirement. Methods of demonstrating system performance included simulating contrast at the 2K level and testing the maximum contrast measurement ability. Both were completed by replacing the 'released'/closed shutter images with opaque or semi-opaque test articles. Switching the closed field of shutters with a 3.3 neutral density (ND) filter simulated a uniform field of 2000 contrast and switching with a 100% opaque material tested maximum measurement ability. Several pinholes were placed randomly in the opaque mask to simulate the regular presence of 'failed opens'. In each case, 'open' shutter measurements were simulated by acquiring images with the shutters simply removed, i.e. acquiring a flat field. ND filter contrast was measured to be less than 5% below the test article's 2K rating, showing the systems measure 2K shutter contrast on the conservative side. A more representative test of systematic error entailed measuring maximum contrast near 'failed opens' simulated by pinholes in the opaque mask. As with normal shutter measurements, a source mask was aligned to block light directly incident on 'failed opens'. Maximum contrast measured adjacent to failed open shutters (blue annuli) was 49K with areas measured away from 'failed opens' averaging at 56K (yellow circles). The calibration results clearly show the MSA test facility capable of accurately measuring shutter contrast as high as 50K, well above the 2K test requirement.

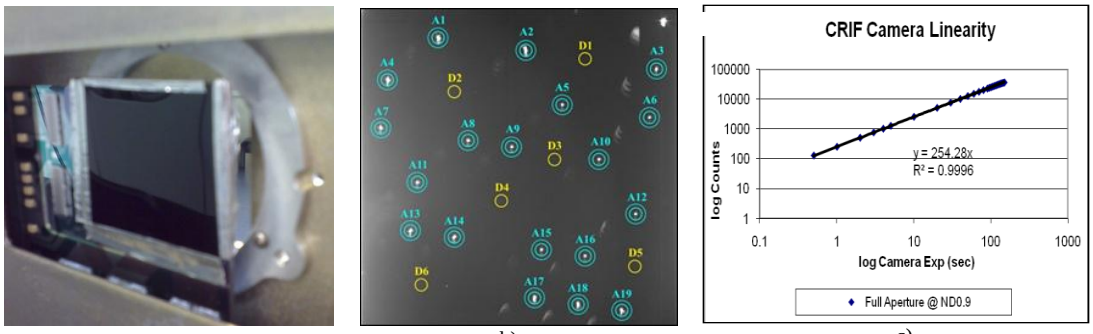

a) b) c)

Figure 6. Illustrations of calibration hardware and results: a) 3.3 ND filter test article to simulate uniform 2K contrast, b) 1000 sec exposure of opaque mask with pinholes to simulate 'failed open' shutters with blue annuli sampling contrast near leaks and yellow circles sampling contrast away from leaks, c) Logarithmic plot of camera counts per second.

4.3 MSA visible and IR contrast results

In addition to MSA facility hardware, a set of software routines was developed to reduce quadrant images to a map of contrast values for each shutter on the array. The software spatially transformed microshutter quadrant images in the open and closed states to account for optical system distortion and scale factor. A ratio of the total signal within the area of each individual shutter was then mapped into an array of contrast values. These routines were applied to measurements taken on flight MSA quadrants Q1-52-102, Q2-42-128, Q3-26-106 & Q4-55-116 in June of 2010. Results were displayed as 2D plots with contrast corresponding to grey-scale values and any shutters below 2K uniquely identified with a color scale. 2D plots of visible and 1.6 μm contrast results are shown in Figure 7. The contrast plots show the relative positions of the four quadrants as they are located on the MSA mosaic base plate (+X to the right as per the axis in Figure 2). In the visible plot, all values above 2K are represented by the grey-scale provided. Groups of failed open shutters are identified by color-coded circles where values below 2K are labeled green, below 1500 are yellow, below 1000 are blue and below 500 are red. Due to the tight scale, several failed open shutters may be present within a single circle.

The high-magnification images in Figure 8 show that leaking shutters are produced by a variety of failure mechanisms. 'Failed opens' labeled in green or yellow are commonly caused by shutter blades not lying flat enough to block all transmitted light. A process of warming and re-cooling the arrays can often reset the contrast of some of these 'border-line' shutters such that some 'failed opens' are recovered. Recoverable shutters are labeled as intermittents and are not included in the results. Red 'failed opens' with contrast below 500 are nearly all caused by broken light shields or by shutter blades getting wedged and twisted in their cells. These failures were prime candidates for plugging as they are not typically recoverable by warming the arrays. Direct comparison of the IR and visible contrast maps in Figure 7 show the degree to which the transmission modes are distinct, as discussed in Section 3.2. The IR plots appear relatively uniform because IR contrast is, to a large degree, spatially independent. Conversely, visible results show an abundance of non-homogeneity across each array. This is in part due to the fabrication process of the quadrants. Quadrant one features three small, low contrast rectangular areas where a trial light-shield design was evaluated. Quadrant two features a unique peripheral ring of low contrast shutters caused by imperfections in the DRIE process and damage incurred by unsynchronized latching. Besides unique features, each quadrant exhibits definite morphology of high and low contrast shutters distributed in a noticeably specific nature. This distribution originates from infinitesimal misalignments of the photolithographic masks during the RIE fabrication process. When the top-side RIE mask that etches the blade shape is not in perfect alignment with the back-side DRIE mask that etches the shutter aperture, the shutter blade is not correctly aligned in its opening. [12] In addition to the obvious risk of damage from blades contacting walls, misaligned shutter blades have the capacity for allowing higher transmission. The result of linear mask misalignment is clearly visible on quadrants 2-4 where shutter contrast gradually decreases from left to right. On each quadrant, the areas of highest contrast are the plugged shutters. High plug contrast adjacent to low contrast shutters confirms the presence of very low stray light and high measurement accuracy.

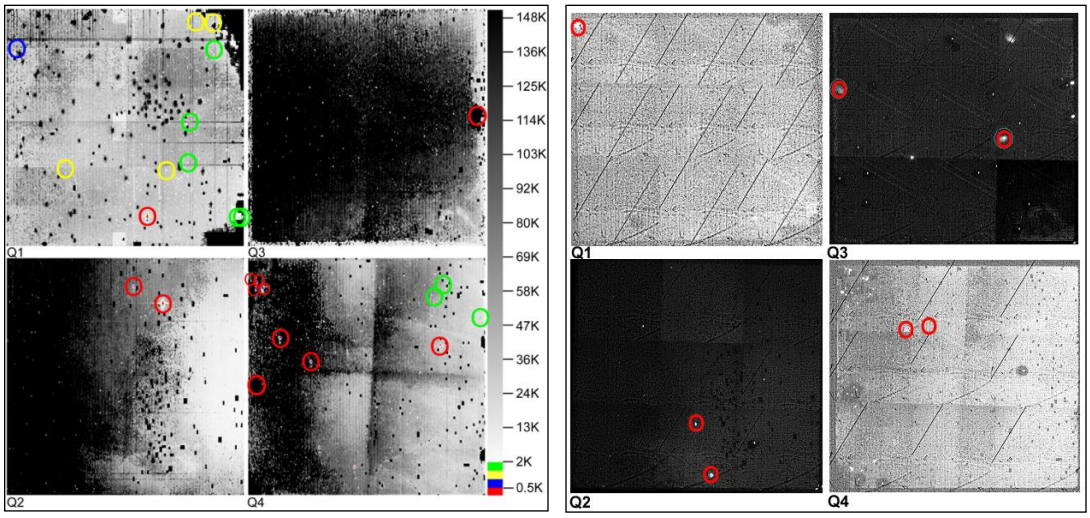

Figure 7. Left image shows visible light contrast maps of the four flight quadrants as they are viewed by the NIRSpec detector. Each pixel in the image represents a single shutter's contrast value in grayscale where shutters below 2K contrast are color coded as per the side scale indicates. To aid visibility of 'failed open' shutters, appropriately colored circles have been added around the failures. The right image shows 1.6 μm (IR) contrast maps (stretched to different grayscales). Red circles denote leaking areas not identified during visible, quadrant-level measurements. Each IR quadrant image is created from a 3 × 3 image mosaic where the slanted lines originate from a single scratch on the IR detector.

There are some additional distinctions between the IR and visible results shown in Figure 7. Notably, the images acquired to produce the 1.6 μm plots were obtained exclusively from the quadrant-level test facilities. After IR contrast was shown to be largely independent of the shutters' performance, further characterization on the MSA structure was deemed unnecessary. Unlike the single images acquired for visible contrast, each IR quadrant image was acquired in nine mosaic tiles and stitched together with custom software.

For visible contrast images, each shutter was resolved and mapped to a single contrast value. The median of the log of these values was used to produce a median contrast value for each quadrant. The size of the IR detector available to us did not permit the same image resolution, falling short of resolving individual shutters. For this reason, average IR contrast values were calculated by measuring groups of larger regions across the arrays. The colored circles on the IR plots denote leaking areas that were not identified during visible, quadrant-level contrast measurements taken immediately prior to the IR measurements. Further analysis was later completed to identify the position and contrast values of these unique IR failures. Their positions were compared directly to the locations of failed opens identified from the MSA-level contrast measurements, showing only one unique IR failure located on quadrant two. The origin of this 'failed open' may be damage to the support structure but it is more likely caused by an intermittently failing shutter blade.

Table 1: Visible contrast results for flight MSA quadrants as of 6/2010. Table provides the total number of shutters under 2000 contrast ('failed opens') and total number of non-opening ('failed closed') shutters on each quadrant. The combined number of failures is within NIRSpec requirements. Average contrast is also presented in the visible and IR and is above the 2K requirement (median is provided due to non-Gaussian distributions).

Quadrant ID	Q1-52-102	Q2-42-128	Q3-26-106	Q4-55-116
Total Failed Open*	24	2	1	18
Total Failed Closed	9,531	5,997	12,087	5,601
Median Vis. Contrast	37,000	102,300	146,400	74,600
Avg. 1.6 μm Contrast	13,400	13,000	16,600	7,600

* Does not include intermittently failing shutters

Our analysis software also generated contrast histograms and tables providing the number of 'failed opens' and 'failed closed' shutters. 'Failed closed' shutters (ones that are permanently stuck closed) are visible in the latched open image of Figure 4. For NIRSpec to achieve its science goals, no more than 5% of shutters may be 'failed closed' and no more than 1% of shutter rows may contain 'failed open' shutters. [11] Numerical results are presented in Table 1 and graphical results are shown in Figure 8. Table 1 shows the performance of the quadrants vary across several aspects with minimal correlation between each characteristic (contrast, number of failures, etc.). Although quadrant three features several thousand additional 'failed closed' shutters, a larger number of 'failed closed' shutters is comparatively acceptable relative to additional 'failed opens'. The histogram in Figure 8 shows peak visible contrast values for each quadrant to be well above the 2K requirement and in two cases, above the 100K goal. These contrast results obtained prior to delivery of the MSA to the NIRSpec bench show the MSA is within its science requirements. The combined number of 'failed closed' shutters and 'failed open' rows was acceptably below the 5% and 1% goals. As of May 2011, our characterization of 'failed opens' provided by this analysis has been used to locate and plug all remaining 'failed open' shutters.

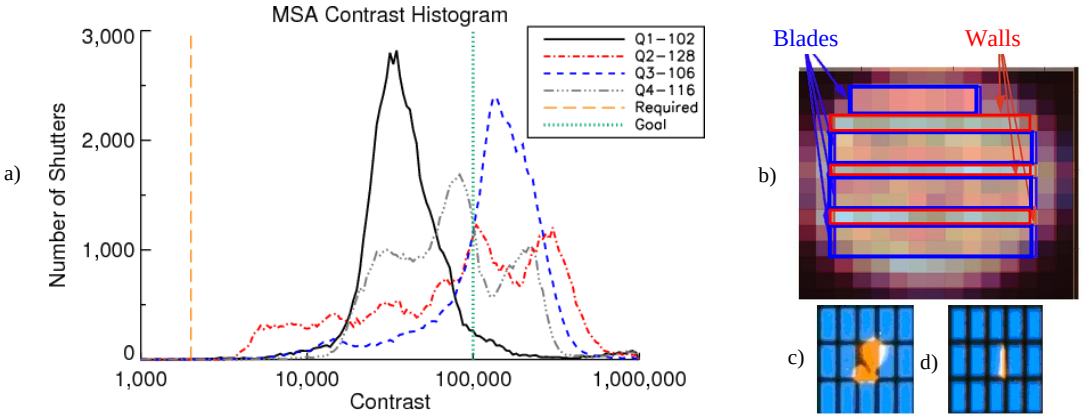

Figure 8. a) Visible contrast distribution of individual shutters on flight quadrants, plotted as a histogram in logarithmic scale. Yellow vertical line indicates 2K contrast requirement, green vertical line denotes 100K contrast goal. b) High magnification image of IR shutter transmission through prototype array (through pinhole to exclude stray light). Blue regions indicate position of shutter blades, red regions indicate positions of non-metalized support structure walls transmitting in the IR (measuring higher counts). Metal wall coatings on the flight quadrant design increased contrast by ~300x, although still allowed some transmission through 2 µm gaps. c) High magnification image of a non-recoverable 'failed open' shutter with shutter blade twisted in cell. d) High magnification image of a recoverable 'failed open' shutter transmitting light past a bowed shutter blade.

5. MSA OPTICAL METROLOGY: ALIGNMENT EVALUATION

5.1 Requirements and test methods

During the cryogenic cycles required to perform MSA contrast measurements, additional optical metrology was performed which entailed optically gauging the position on the shutter arrays to define their cryogenic position and ensuring their stability within their operating temperature range. Shutter stability is essential to avoid spectro-photometric errors in NIRSpec's observations. [13] In addition to measuring contrast, the MSA evaluation facility is designed to perform non-contact photogrammetry measurements. The measurements are capable of precisely determining each quadrant's motion in six degrees of freedom with respect to a centralized optical reference frame (ORF). The alignment requirements are as follows:

Positional knowledge must be measured to ± 5µm in the X, Y and Z (focus) directions between the ORF and quadrants at ambient and at 30K. Cryogenic offset between the ORF and each sub-array in the X, Y and Z directions must be no more than ± 100µm. The stability requirement between the ORF and the quadrants is ±10µm in Z and ±1µm in the X-Y plane within the operational temperatures range of 30-40K. Stability must also be maintained across periodic 260K heat cycles in order to release intermittently stuck shutters. To avoid frequent recalibration of NIRSpec, shutters must

maintain their stability requirement over several thermal cycles. Confirming these requirements entailed measuring the relative movement between the ORF and quadrants before and after four heat cycles.

The ORF is defined as the center of the field of shutters where NIRSpec's boresight will be located. For the purpose of our measurements, we define the ORF as the center of the cruciform hardware directly past this location in focus. Alignment images were acquired with our camera and illumination systems centered on the middle of the cruciform. In this manner, both the centralized ORF is visible as well as the inner shutter fields of all four quadrants, as shown in Figure 9c. Early measurements encountered imaging problems involving illumination, focus and insufficient magnification. Poor sampling of defocused targets provided system measurement accuracy in the four micron range, inadequate to meet our one micron stability requirement. Measurement of cryogenic, sub-micron motion required optimizing new pattern recognition software with additional optical hardware. Improvements included camera-side illumination and optics customized for the field of view.

5.2 Imaging and system automation

Figure 5 shows the location of additional camera-side LEDs used to front-light the MSA for performing alignment and stability measurements. The off-angle LED arrays provided a dark-field illumination that enhanced the contrast of specific features in the field of view, thus simplifying the analysis process. Our alignment metrology plan was initiated by acquiring sets of images at ambient temperatures (293 K), prior to cool-down. Analysis of these images to accurately determine quadrant-to-cruciform motion depended on the presence of sharply focused features. Measuring relative motion between the cruciform (indicating the ORF position) and a quadrant required compensating for the 1mm of defocus between the non-coplanar cruciform and quadrant surfaces. Retardation plates were used to refocus selected areas of the image field, bringing all regions into simultaneous optimal focus. A retardation plate fixture was mounted directly in front of the CCD camera and aligned such that the glass retarded the focus of quadrant surfaces only. The fixture shown in Figure 9a is constructed of 4 glass plates of a thickness designed to produce the required amount of change in focus. Prior to cool down, large sets of images were acquired through the plate fixture of both the central field shown in Figure 9c as well as the outside quadrant corners. After ambient images were acquired, the retardation plates were used during cool down to keep track of the ± 100 micron limited quadrant movements with respect to the ORF.

During four 18-hour cool downs, the MSA hardware would contract and change position. To compensate for this, camera stage positions were controlled with machine vision software programmed to keep the cruciform focused and centered in the camera's field of view. Image tracking was essential to reduce parallax errors between the non-coplanar shutters and cruciform. Tracking was accomplished by scheduling automated focus sweeps and image acquisitions at specific MSA temperatures. The automated focus routine captured series of images at varying focal distances from the cruciform. From these images, image processing measured image sharpness, fitted a Gaussian curve to the sharpness data and then moved the camera to the optimal fixed focal distance from the cruciform. Through this method, focus was repeatable to ±10 microns. After best focus was located, a second software routine moved the camera to center the focused cruciform surface pattern within the camera field of view; thereby aligning the camera in a repeatable position with respect to the cruciform. The combination of both routines provided automated camera tracking of the MSA hardware as it contracted and moved during cool downs. Although camera position was limited by stage accuracy, alignment was still accurate and repeatable to less than one camera pixel, thereby minimizing parallax-induced errors.

By recording the stage positions in the image file headers, quadrant motions were tracked during the entire cool-down. Once a stable operating temperature was reached, a set of 30 center-field images was acquired before repeating the process for images of the outside quadrant corners. The center-field image shown in Figure 9c identifies regions used for measuring quadrant-cruciform offsets during cool-down. The colored boxes indicate regional templates selected for focus and image registration analysis: 80 shutter regions in green, 80 cruciform regions in blue and 272 (tiny) regions along the quadrant edges in red. Registration analysis was completed on red regions featuring microscopic chevron-fiducials printed at the edges of the arrays adjacent to the shutters and on textured regions of the cruciform surface (blue boxes). Results yielded motion in the X-Y plane and about the Z direction. Focus analysis was completed on the same blue cruciform regions as well as the regions of shutters labeled in green boxes. Focus results yielded motion in the Z direction and about the X and Y directions (tip and tilt). The images acquired at the outside array corners aided the

accuracy of quadrant rotation analysis. In general, better-focused and finely illuminated target regions produced quadrant motion results within two micron accuracy. This accuracy was sufficient for determining cryogenic offsets to within the ± 100µm offset requirement.

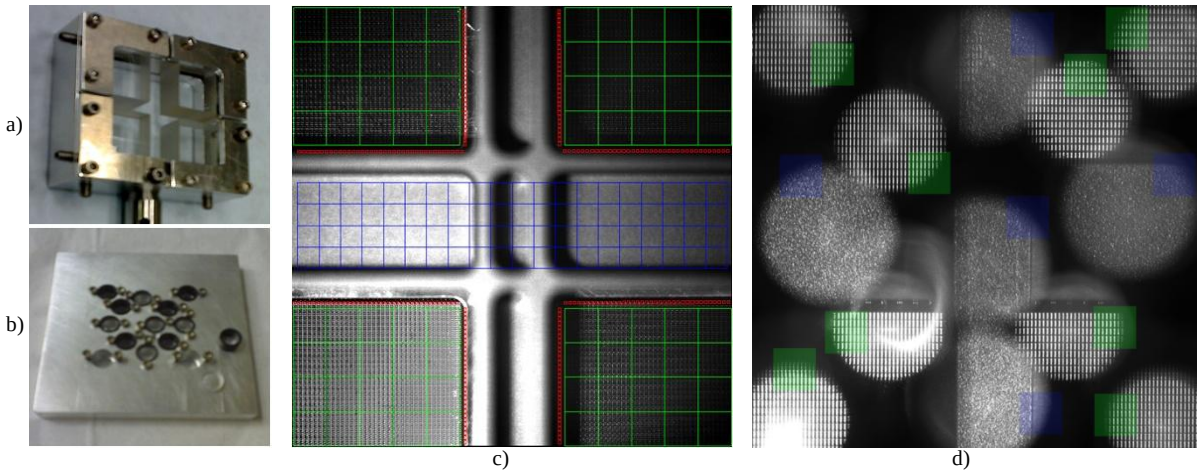

Figure 9. a) Photo of retardation-plate fixture used for brining non-coplanar cruciform and shutter fields into same focus. c) Focus-corrected center-field image of cruciform and quadrants through retardation plates (showing inner corners of quadrants only or ~1/3 of full field). b) Photo of mini-lens fixture used for magnifying selected portions of the image field for stability analysis. d) Focus-corrected center-field image of cruciform and quadrants through mini-lens fixture. Red, green and blue boxes indicate regions selected for image registration analysis.

Although retardation plates worked well enough for cryogenic offset measurements, better than 1:1 magnification was required to satisfy the ± 1µm MS stability requirement. A 'minilens' assembly of 13 miniature lenses was fabricated to magnify selected portions of both the quadrants and the cruciform and mounted in place of the retardation plates. The assembly shown in Figure 9b shows five lenses positioned for magnifying cruciform targets and two lenses located over each of the four quadrants. The resulting image shown in Figure 9d illustrates magnified target regions at various distances from the ORF. The colored regions were selected for image registration analysis: 8 shutter regions in green and 5 cruciform regions in blue. Each lens provided a 3X magnification for these areas, improving the image sampling resolution to three microns per pixel from nine microns per pixel. Selective image region magnification combined with analysis software improved the accuracy of the measuring hardware stability to better than one micron. The quadrants' stability was measured over 4 heat cycles to 260K, with images acquired at 30K after every two cycles. The process for acquiring stability data images was altered to include finer focus adjustment sweeps. Image tracking was also discontinued in order to remove stage position errors from the measurements.

5.3 Image registration analysis methods

Improvements to the MSA facility's hardware provided well-focused targets for photogrammetrical image analysis. A variety of image registration algorithms were considered for the analysis of shutter alignment. These algorithms determine the geometric transformation required to align a pair of images.[14, 15] We applied two different image registration algorithms on various cruciform and quadrant regions that were extracted from our mini-lens images, similar to those shown in Figure 9d, before and after cryogenic cycles. Both image registration algorithms were applied during ETU metrology in order to minimize potential processing errors by comparing the results obtained from each approach. One algorithm used was a standard pattern-matching function from National Instrument's Labview add-on Vision toolkit. [15] This function performed a normalized cross-correlation method to find instances of the mini-lens regions, or templates, within the search image. Normalization, performed by the function, made the processing less sensitive to image brightness changes due to lighting and exposure conditions. The normalization is an implementation of the Pearson product-moment correlation coefficient. It is done by subtracting the mean and dividing by the standard deviation of the template and search region at each convolution step. Typically, cross-correlation methods require a lot of processing calculations. For our application, the amount of processing was limited because camera alignment routines were successful in pre-aligning the camera prior to acquiring images. As a result, template shift, scaling, and rotation

were well known. The high-precision processing was quick for search regions only a few pixels larger than the mini-lens templates. Vision's Toolkit documentation describes this correlation method as follows: *Consider a sub-image w(x, y) of size K × L within an image f(x, y) of size M × N, where K ≤ M, L ≤ N and the origin of the image f is at the top left corner (*as shown in Figure 10*). Correlation is the process of moving the template or subimage w around the image area and computing the value C in that area. This involves multiplying each pixel in the template by the image pixel that it overlaps and then summing the results over all the pixels of the template. The maximum value of C indicates the position where w best matches f. The correlation between w(x, y) and f(x, y) at a point (i, j) is given by* [15]

$$C(i,j)=\sum_{x=0}^{L-1}\sum_{y=0}^{K-1} w(x,y)f(x+i,y+j) \quad \text{where} \quad \begin{matrix} i=0,1,\ldots M-1 \\ j=0,1,\ldots N-1 \end{matrix} \tag{2}$$

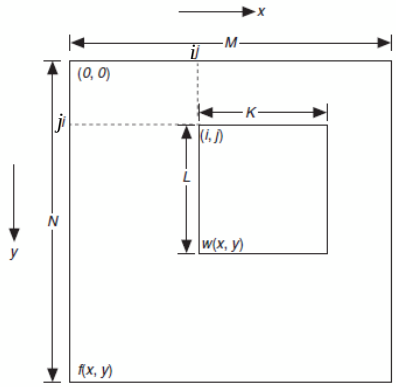

Figure 10. National Instrument's cross-correlation method demonstrated by multiplying overlapping pixels of subimage w within image f. The position where w best matches f is found by identifying the largest sum of multiplied pixels within the template.

The other algorithm used was a coarse-to-fine wavelet-based pyramid algorithm originally developed by Thevenaz, Ruttiman, and Unser (TRU) [16, 17] for registering 3-dimensional medical images, and modified at the Goddard Space Flight Center for registering large 2-dimensional remotely-sensed satellite images. [18] TRU relies on wavelet decomposition of 2D images into low-to-high frequencies, similar to Fourier transforms. In a wavelet representation, the original signal is filtered by the translations and the dilations of a basic function, called the "mother wavelet". Equation 2 shows the general continuous form of a wavelet transform of an image *I*,

$$Wav(I)(a,b)=\frac{1}{\sqrt{a}}\int_{-\infty}^{\infty}\int_{-\infty}^{\infty} I(u,v).W\left(\frac{u-b_1}{a},\frac{v-b_2}{a}\right)d_u d_v \tag{3}$$

where *W* represents the "mother wavelet", $b=(b_1, b_2)$ is the translation factor and *a* is the dilation factor. All the dilations and translations of the mother wavelet form an orthonormal basis in which the function image is uniquely represented and therefore the transformation can be inverted to produce the original images from the unique representation. [19] The images are filtered in a multi-resolution process starting with low-accuracy, low-resolution features before iterating to high-frequency and highly accurate spatial features (a pyramidal approach). In this manner, low-pass features like cruciform structure provide rough registration before high-pass features like small shape edges provide the fine-accuracy registration. For high-accuracy measurements, it was therefore essential for selected analysis regions to contain high-frequency spatial features such as the quadrant chevron-fiducials and cruciform texture. Thirteen 512 × 512 pixel regions of each image were selected for registration, from which the motion of each quadrant was calculated by averaging the motions of matching inner and outer regions (Figure 9d). This method performed similarly to the National Instruments method, worked best for regions containing large and small object features, and required

little operator inspection. Both algorithms were applied to regions extracted from batches of 30 successive high-resolution images to compare movements of different regions within the images against their corresponding regions in the first baseline image. Both also employed automatic region registration that enabled unsupervised batch registration of multiple images. This was particularly useful as over 1000 images were analyzed during stability cycles alone. Ultimately, the two algorithms yielded near-identical stability measurements that were indistinguishable from the two-sigma noise floor of 0.3 microns, or $1/10^{th}$ of a pixel.

For flight hardware metrology, each algorithm was selectively applied to data sets that corresponded to its optimal performance on the ETU hardware data. Use of the TRU algorithm was limited to analysis of X & Y motion during 30K stability cycles only. This was due to the algorithm requiring stable shutter fields. TRU was not applied to the analysis of cool-down data since the position of shutter reflections would typically change due to shutter blades bowing at warmer temperatures. Results also contained registration errors whenever the uniform pattern of shutters shifted by more than one grid cell. Analysis of motion in the Z and R_Z directions through stability cycles was completed with the National Instruments (NI) algorithm. The NI method was also exclusively used for analysis of the flight hardware cryogenic offset images (determining quadrant motion during cool-downs). During cool-downs, the NI algorithm extracted 80 shutter regions, 80 cruciform regions and 272 quadrant-edge regions (Figure 9c) from over 4000 images. Offset results were obtained from evaluating the motion of these regions with respect to the first ambient reference image. Groups of 30 images were acquired at a time to provide measurement error and 'knowledge' of quadrant position. To determine stability across each cryogenic cycle, results were obtained from evaluating the position of 13 mini-lens regions (Figure 9d) selected from 30 sequential images. The 30 images were individually processed to determine the average position of quadrant regions with respect to the average position of cruciform regions. Image results were then averaged together among groups of 30 images to reduce random noise effects. The calculated position of the quadrants with respect to the cruciform was then averaged across four sequential cryogenic cycles. Finally, the four-cycle average was subtracted from each individual cycle to assess stability. The deviation of individual cycles was then compared to the 1 micron stability requirement. Error from stage motion was excluded by using a single, central stage location to acquire images throughout stability cycles. Focusing routines employed exclusively prior to, and after, stability cycles provided stability data in the Z direction.

5.4 Results of image registration analysis for shutter alignment

Image registration algorithms were successfully used to determine the motion of the microshutter quadrants with respect to the NIRSpec boresight (ORF). Quadrant motion from cryogenic offsets and stability within operating temperatures were satisfactorily measured in six degrees of freedom. The alignment results presented in Table 2 and Figure 11 show the motion of the quadrants is well behaved during cool-down. Each quadrant contracts towards the ORF as predicted by thermal models. Larger motion in the Y and Z directions is due to the quadrant's substrate deflecting from hardware designed to secure it exclusively at ambient temperatures. The relatively larger motions in the Y and Z directions contributed towards higher measurement error and reduced knowledge of final Y, Z and Rz positions. Positional knowledge in focus (Z) was also frustrated by dependency on limited stage readout accuracy. Results from positional knowledge about the X and Y directions also show analysis of quadrant rotations contained greater measurement error. This is due to calculation of rotation being dependant on the focus routine's ability to find best focus at outer quadrant locations. Rotational measurement precision was largely determined by the focus sampling interval (i.e. the Z distance between each image). Sampling intervals were not high enough to achieve the requisite level of rotational measurement error. Requirement waivers were requested for positional knowledge by the GSFC MS team and subsequently granted by NIRSpec/ESA.

Table 2: Quadrant alignment results from DVI and TRU image registration algorithms over multiple cryo-cycles (4 cryogenic offset cycles on left and 4 stability cycles on right). The TRU algorithm is used for X and Y stability only. Linear units are in microns (X, Y, Z) and rotations are in microradians (R_X, R_Y, R_Z). Listed stability results are zero-to-peak. Results show all cryogenic motion of flight quadrants is within spec with knowledge of cryogenic offset below requirement accuracy. Positions are in microns, rotations are in micro-radians.

Offset	X	Y	Z	R_X	R_Y	R_Z	Stability	$X^{\dagger}$	$Y^{\dagger}$	Z	R_X	R_Y	R_Z^{*}
Q1	8	26	7	-44	29	443	Q1	0.2	0.5	8			8
Q2	5	-45	-14	6	20	-355	Q2	0.2	0.3	6			10
Q3	-6	20	21	-2	-10	-219	Q3	0.2	0.7	5	*12*[ETU]		10
Q4	-3	-36	-11	32	-34	414	Q4	0.2	0.3	1			10
Req.	±100	±100	±100	±500	±500	±500	Req.	±1	±1	±10	50	50	10
Knowledge	±5	±15	±25	±110	±110	±100							
Req.	±5	±5	±5	±50	±50	±50							

† Results from TRU algorithm

* Start to finish comparison (before 1st cycle to after last cycle)

ETU ETU test results; not feasible on flight hardware

The stability results presented in Table 2 and Figure 11 demonstrate that each quadrant retains its position across four 260K heat cycles. As the table shows, neither algorithm provided results for rotation about the X and Y directions (R_X & R_Y). A limitation of using mini-lens images was the relatively short ~2mm distance between analysis regions on each quadrant (green areas in Figure 9d). Attempting to distinguish variance in focus between the two areas with a measurement accuracy of ±10 microns was insufficient to meet the tight rotational requirement. However, quadrant R_X and R_Y were earlier established to be within requirements by means of theodolite metrology performed on modifiable ETU hardware. Figure 11 shows X (dispersive direction) and Y (cross-dispersive direction) offset results from the NI algorithm and stability results from TRU. The relative motions between each quadrant and the ORF are plotted across several cryogenic cycles. The offset plots feature arrows indicating the direction of the quadrants' motion with respect to the ORF. It is clear that both X and Y cryogenic offsets are well within the 100 µm requirement for each of the four quadrants. Stability within the operating temperature range is also well within the 1 µm requirement and remains so over several heat cycles to 260K. Average stability in the X-Y plane was found to be 0.45µm from TRU results, with system measurement accuracy of 0.3µm.

The 0.3µm measurement accuracy of the MSA facility was both exceptional and partially predictable. Standard image processing algorithms were expected to yield roughly 1/5th of a pixel (0.6 micron) precision. Differencing positions relative to a starting point increased noise by a factor of the square root of two. Differencing positions a second time, from array to cruciform, increased noise by another square root of two. Averaging across the 30-image set, reduced the noise by a factor of 5 (i.e. 1/(square root of 30)). Factoring all of this together, the expected image processing performance, without accounting for systematic drifts, was about 0.07 pixel, or 0.2 micron. During stability measurements, a strong diurnal temperature drift was observed within the test facility. To minimize effects of temperature drift, measurements were taken at the same time of day, and ambient temperature was recorded in the image headers. The systematic temperature drift, likely accounted for another 0.1 micron of uncertainty. Similar average results of 0.5µm were obtained from ETU hardware, demonstrating that quadrant motion showed no clear trend over an extensive 20 stability cycles. Our results indicate microshutters are stable to within 0.5µm, or one sixth of a pixel's resolution, with a unique measurement accuracy level of 0.3µm for cryogenic metrology. Based on these results, NIRSpec will acquire spectra devoid of source mask-induced spectro-photometric errors.

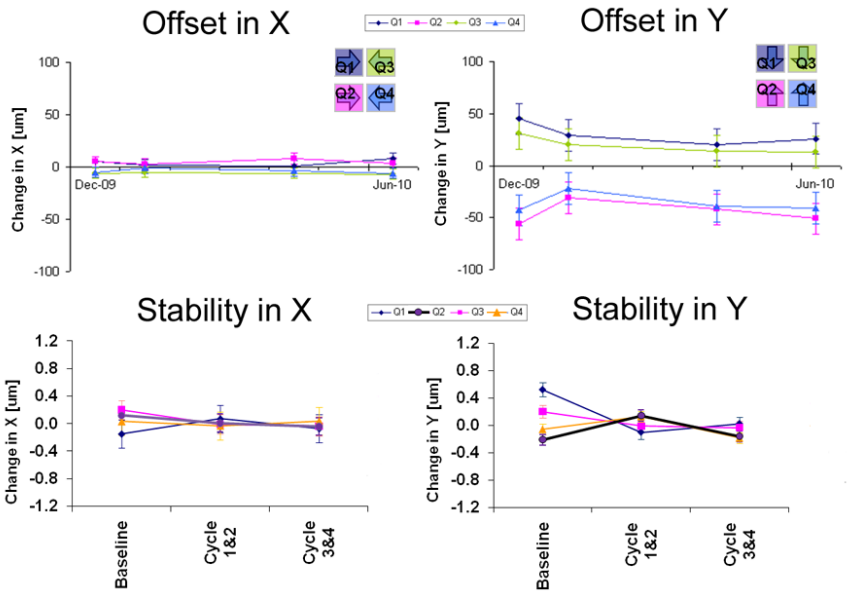

Figure 11. Plots of cryogenic offset and stability within the operating temperature range for the four flight quadrants. Offset results are provided by NI and stability results are provided by TRU. Arrows indicate direction of quadrant motion during cool-downs. Offset results are shown to be within the 100 µm requirement and stability results are shown to be within the 1 µm requirement.

6. SUMMARY

An extensive test program completed at NASA's Goddard Space Flight Center (GSFC) has demonstrated that the flight microshutter assembly includes focal-plane object selectors that are both high contrast and cryogenically stable. Several facilities were assembled to evaluate the electrical, optical and mechanical performance of all 249,660 shutters individually. Optical results identified all shutters with contrast below 10^4 for repair and demonstrated that average shutter contrast far exceeds the 10^4 requirement. This level of performance confirms that the NIRSpec instrument will be adequately efficient to meet JWST's goal of observing 2500 galaxies in five years. Efforts made to characterize cryogenic motion of the shutters were also successful. Results indicated that microshutters are stable to within 0.5µm and contract from ambient position in a predictable and repeatable manner. Our metrology efforts were based on high-resolution imaging optimized with a creative use of automated image registration algorithms. In the course of flight alignment metrology, over 5000 images were acquired for analysis. The use of photogrammetric methods to obtain non-contact, sub-micron measurements in cryogenic conditions is both unique and novel. Stable and predictable shutter positions will ensure that spectra acquired by NIRSpec will be accurate. Long-term shutter stability across periodic heat cycles will ensure costly time is not lost in repeating spectrograph calibrations.

ACKNOWLEDGMENTS

Optical metrology completed on the MSA structure and during quadrant qualification was successful due to the contributions of several partners and collaborators. Particular thanks go to Peter Blake and Tim Madison for optical design and support, Wayne Landsman and Jacqueline Le Moigne for analysis support, David Rapchun and George Hilton for cryogenic design and support, and David Franz and Christian Zincke for electrical and functional support. The microshutter mission is managed by NASA and the European Space Agency which is in charge of the NIRSpec instrument.

REFERENCES

[1] H.S. Stockman, The Next Generation Space Telescope: visiting a time when galaxies were young, The Association of Universities for Research in Astronomy, Inc., 1997.

[2] J. Samuel H. Moseley, A. S. Kutyrev, R. K. Fettig, C. W. Bowers, R. A. Kimble, J. Orloff, and B. E. Woodgate, "Programmable two-dimensional microshutter arrays," Miniaturized Systems with Micro-Optics and MEMS 3878(1), pp. 392–397, SPIE, 1999.

[3] R. F. Silverberg, R. Arendt, D. E. Franz, G. Kletetschka, A. Kutyrev, M. J. Li, S. H. Moseley, D. A. Rapchun, S. Snodgrass, D. W. Sohl, and L. Sparr, "A microshutter-based field selector for JWST's multi-object near infrared spectrograph," Infrared Spaceborne Remote Sensing and Instrumentation XV 6678(1), p. 66780Q, SPIE, 2007.

[4] W. Posselt, W. Holota, E. Kilinyak, G. Kling, T. Kutscheid, O. L. Fevre, E. Prieto, and P. Ferruit, "NIRSpec- Near Infrared Spectrograph for the JWST," Proc. SPIE 5487, pp. 688–697, 2004.

[5] A. S. Kutyrev, R. Arendt, S. H. Moseley, R. Boucarut, T. Hadjimichael, M. D. Jhabvala, T. King, M. J. Li, J. Loughlin, D. Rapchun, D. S. Schwinger, and R. F. Silverberg, "Programmable Microshutter Arrays for the JWST NIRSpec: Optical Performance," IEEE Journal of Selected Topics in Quantum Electronics 10, pp. 652–661, 2004.

[6] P. Jakobsen, S. Arribas, T. Beck, S. Birkmann, T. Boeker, A. Bunker, S. Charlot, G. De Marchi, P. Ferruit, M. Franx, R. Maiolino, H. Moseley, J. Muzerolle, B. Rauscher, M. Regan, H. Rix, M. Sirianni, D. Soderblom, J. Tumlinson, J. Valenti, and C. Willott, "NIRSpec, The Near-IR Multi-object Spectrograph For JWST," American Astronomical Society, AAS Meeting #217, Vol. 43, 2011

[7] J. P. Gardner, J. C. Mather, M. Clampin, R. Doyon, M. A. Greenhouse, H. B. Hammel, J. B. Hutchings, P. Jakobsen, S. J. Lilly, K. S. Long, J. I. Lunine, M. J. McCaughrean, M. Mountain, J. Nella, G. H. Rieke, M. J. Rieke, H. Rix, E. P. Smith, G. Sonneborn, M. Stiavelli, H. S. Stockman, R. A. Windhorst, and G. S. Wright, "The James Webb Space Telescope," Space Science Reviews 123, pp. 485–606, 2006.

[8] R. K. Fettig, J. L. Kuhn, J. Samuel H. Moseley, A. S. Kutyrev, J. Orloff, and S. D. Lu, "Some aspects on the mechanical analysis of microshutters," Materials and Device Characterization in Micromachining II 3875(1), pp. 210–220, SPIE, 1999.

[9] M. J. Li, I. S. Aslam, A. Ewin, R. K. Fettig, D. Franz, C. Kotecki, A. S. Kutyrev, S. H. Moseley, C. Monroy, D. B. Mott, and Y. Zheng, "Fabrication of Microshutter Arrays for Space Application," in MEMS Design, Fabrication, Characterization, and Packaging, Proceedings of SPIE 4407, 2001

[10] M. J. Li, et al., "Fabrication of Microshutter Arrays for Space Application", in Microelectronic and MEMS Technologies, Proceedings of SPIE 4407, 2001.

[11] A. S. Kutyrev, N. Collins, V. J. Chambers, S. H. Moseley, and D. Rapchun, "Microshutter arrays: High contrast programmable field masks for JWST NIRSpec." in Space Telescopes and Instrumentation 2008: Optical, Infrared, and Millimeter., ser. SPIE, J. M. Oschmann Jr., M.W. M. de Graauw, and H. A. MacEwen, Eds., vol. 7010, pp. 70103D–1:10, 2008.

[12] M. J. Li, T. Adachi, C. Allen, S. Babu, S. Bajikar, M. Beamesderfer, R. Bradley, K. Denis, N. Costen, A. Ewin, D. Franz, L. Hess, R. Hu, K. Jackson, M. Jhabvala, D. Kelly, T. King, G. Kletetschka, A. Kutyrev, B. Lynch, T. Miller, H. Moseley, V. Mikula, B. Mott, L. Oh, J. Pontious, D. Rapchun, C. Ray, K. Ray, E. Schulte, S. Schwinger, P. Shu, R. Silverberg, W. Smith, S. Snodgrass, D. Sohl, L. Sparr, R. Steptoe-Jackson, V. Veronica, L. Wang, Y. Zheng, and C. Zincke, "Complex MEMS device: Microshutter Array System for Space Applications," in Micro (MEMS) and Nanotechnologies for Defense and Security, T. George and Z. Cheng, eds., Proc. SPIE 6556, pp. 716–731, 2007.

[13] M. te Platea, W. Holotab, W. Posseltb, J. Köhlerc, M. Melfb, G. Bagnascoa, and P. Marenacia, "Opto-mechanical design of the Near Infrared Spectrograph NIRSpec," Cryogenic Optical Systems and Instruments XI, Proceedings of SPIE 5904, 2005

[14] J. Le Moigne, N. S. Netanyahu, and R. D. Eastman. *Image Registration for Remote Sensing.* Cambridge University Press, Cambridge, UK, 2011.

[15] National Instruments Corporation. NI Vision Concepts In-Depth Discussion of Cross-Correlation, 2011. [Online] Available from: http://zone.ni.com/reference/en-XX/help/372916L-01/nivisionconcepts/pattern_matching_indepth/ [Accessed 5 Jan 2012].

[16] P. Thevenaz, U. E. Ruttiman, and M. Unser, "A Pyramid Approach to Sub-pixel Registration Based on Intensity," IEEE Transactions on Image Processing, vol. 7, no. 1, pp. 27–41, January 1998.

[17] M. Unser, A. Aldroubi, and M. Eden, “The L2-Polynomial Spline Pyramid,” IEEE Transactions on Pattern Analysis and Machine Intelligence, vol. 15, no. 4, pp. 364–379, April 1993.
[18] I. Zavorin and J. Le Moigne, “Use of Multiresolution Wavelet Feature Pyramids for Automatic Registration of Multisensor Imagery,” IEEE Transactions on Image Processing, vol. 14, no. 6, pp. 770-782, June 2005.
[19] N. Memarsadeghi, J. Le Moigne, P. N. Blake, P. A. Morey, W. B. Landsman, V. J. Chambers, and S. H. Moseley, “Image Registration for Stability Testing of MEMS,” in Computational Imaging IX, SPIE-IS&T Electronic Imaging, Proceedings of SPIE 7873, 2011

Cryogenic Photogrammetry & Radiometry for the James Webb Space Telescope Microshutters

John Chambers
MSS Optical PDL
1 July 2012

Overview

- **Introduction to NIRSpec and Microshutters**
  - Science Requirements & Objectives
  - Microshutters and subsystem design
- **Test Objectives and Measurement Methods**
- **Design of Subsystem Evaluation Facility**
- **Microshutter Contrast Test Results**
  - Contrast Measurements (Visible Band)
  - Contrast Measurements (IR Band)
- **Characterizing Shutter Motion via Photogrammetric Sub-pixel Image Analysis**
  - Results of measuring cryogenic offsets of quadrants during cool-down (290K - 33K)
  - Results of measuring cryogenic stability of quadrants through operating temperatures (33K - 260K)
- **Conclusions**

Optical Layout of JWST /NIRSPEC

Optical Telescope (OTE)

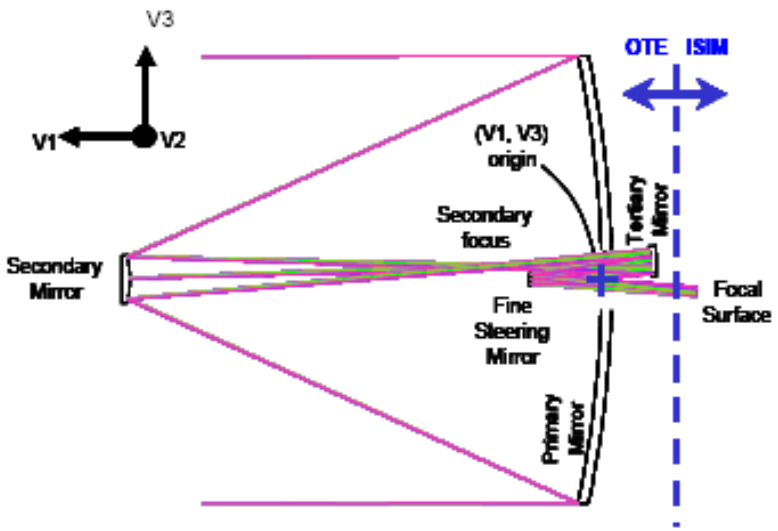

NIRSpec Optics

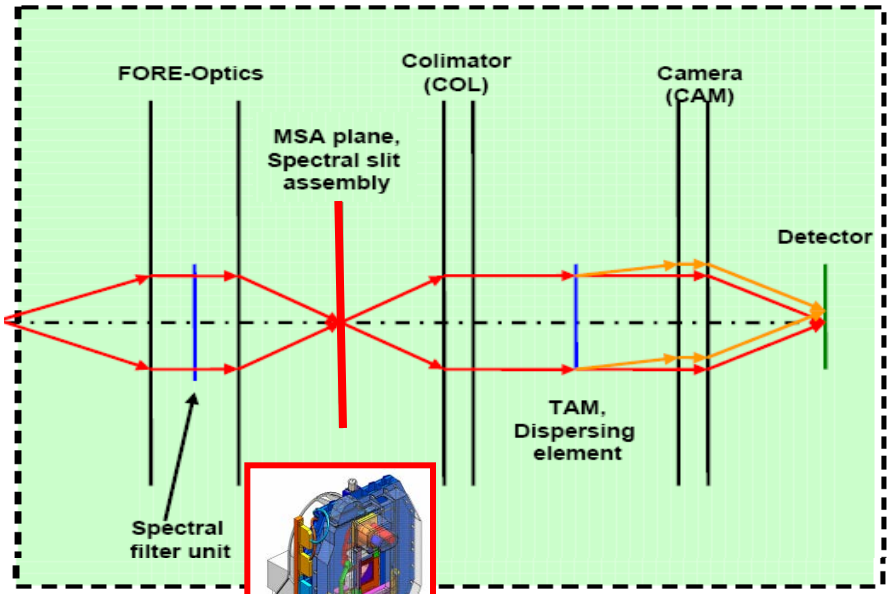

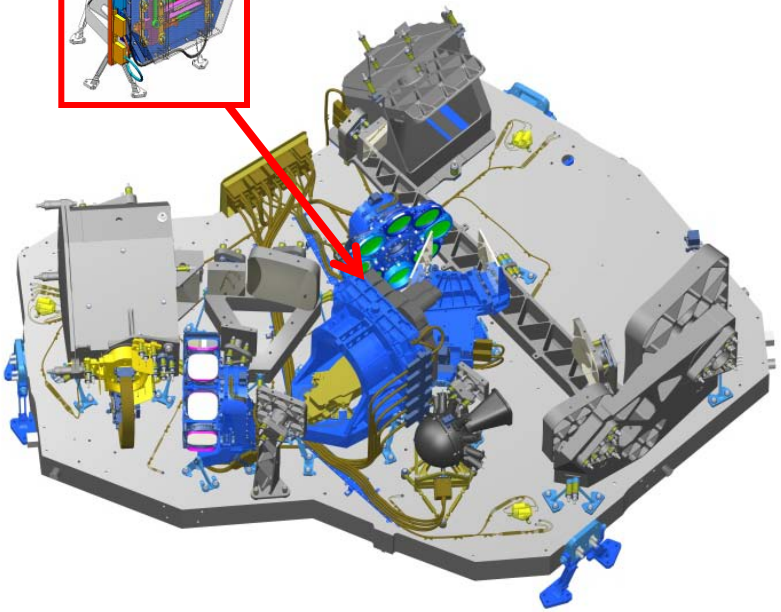

Science Requirements & Objectives

- **Measure the spectra of at least 2500 galaxies within the 5 year mission's observing time**
  - The NIRSpec shall enable multi-object spectroscopy of up to 100 objects simultaneously
- **Microshutter arrays: a controllable and reconfigurable aperture mask that permit faster mapping and cataloging of faint infrared objects**
  - Shutters are the only solution to produce high contrast ratios required by NIRSpec: **The Open-Closed contrast of the shutters shall be > 2000 with a goal of >10^5** in order to avoid having target spectra be polluted with the light from other nearby or bright sources in the same field of view
  - Precise selection of diffraction-limited targets **requires field selectors that are stable to within 1 micron**
  - In order to avoid clipping of the sources, it is essential to ensure that the MSA is stable in six degrees of freedom at 35K
  - Alignment requirements for the microshutter arrays include defining their cryogenic displacement, knowledge of their position at operating temperature and stability of their position across the operational temperature range.

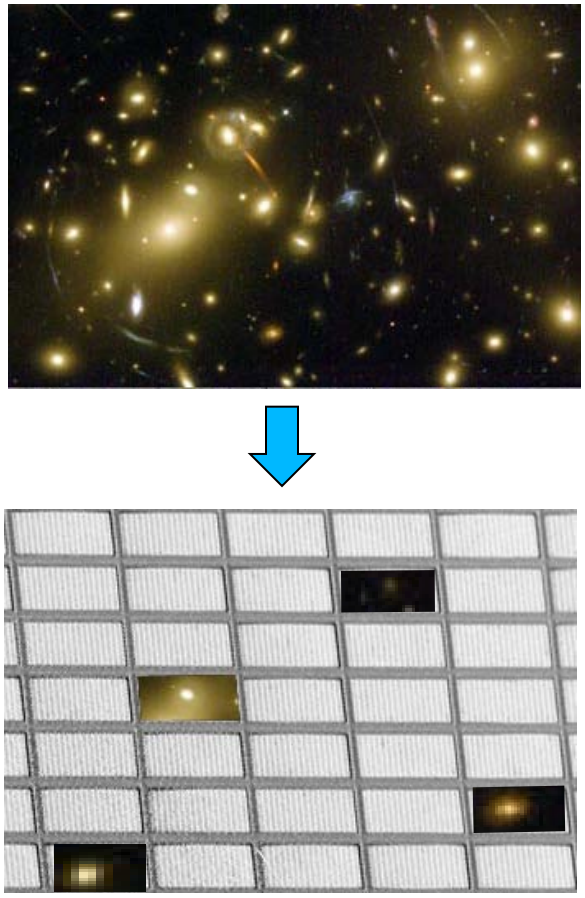

Microshutters Design

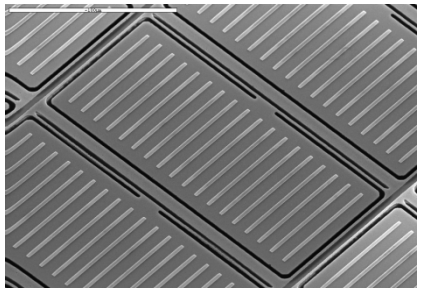

Individual Shutter

100 x 200 microns

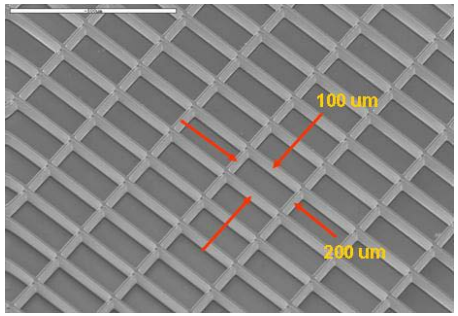

Backside of Array

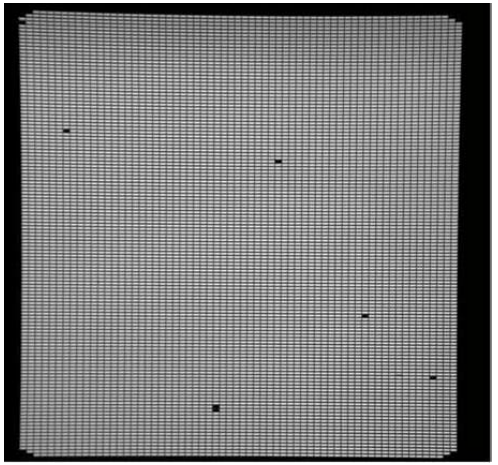

171 X 365 Array

62,415 shutters

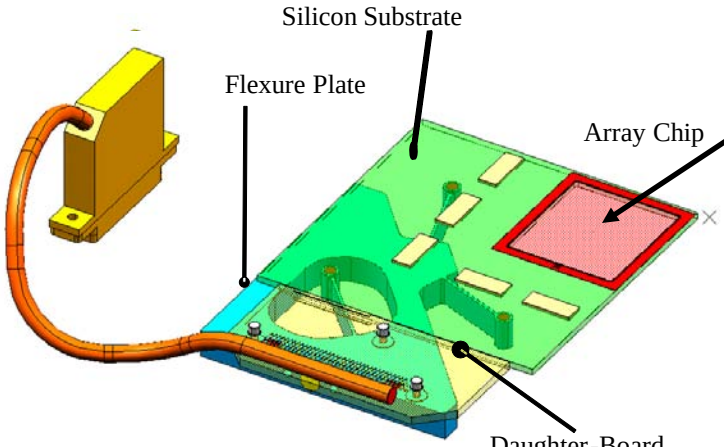

Quadrant

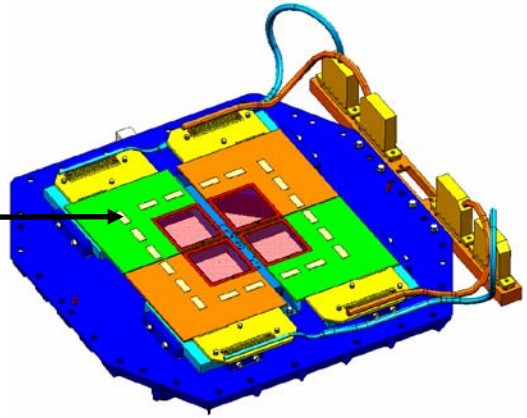

Flight Mosaic

Assembly of 4 Quadrants

Microshutters Sub Assembly (MSA) Design

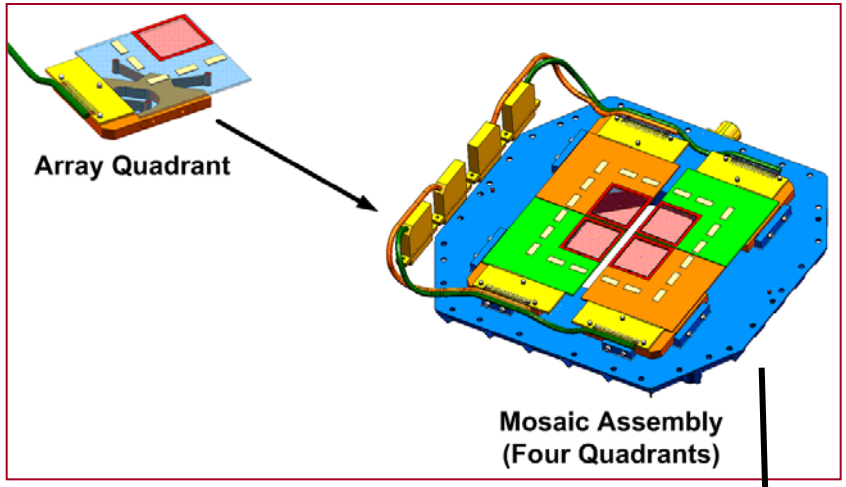

- MSA is comprised of four array quadrants of 365 by 171 shutters assembled onto a base plate via titanium flexures
- Center of 4 quadrants is titanium ‘cruciform’ structure with optical ref. frame (ORF)
- Tested with MSA evaluation facility
  - Measures array contrast
  - Measures alignment at ambient & cryogenic temperatures

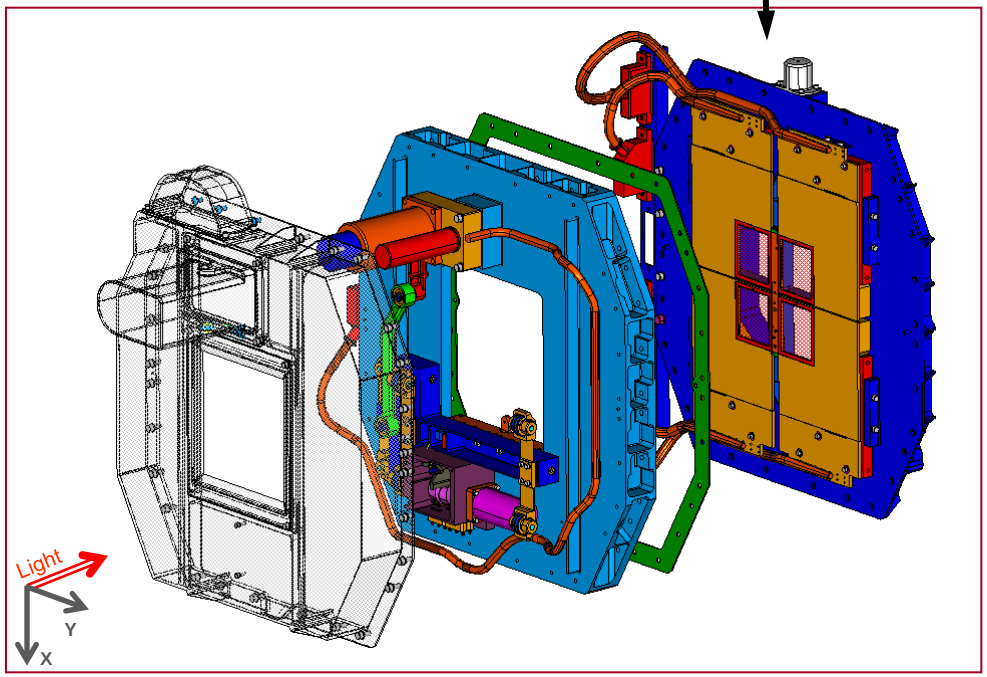

Camera/NIRSpec Side

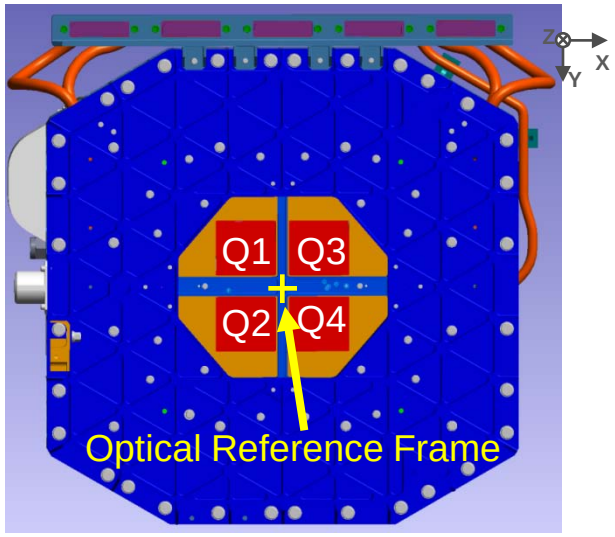

Objectives and Measurement Methods

- **Test Objectives**
  - To measure the visible (630nm) and infrared (1.6 μm) contrast of 4 flight quadrants
  - To measure the cryogenic offsets (290-33K) of all 4 quadrants with respect to the ORF in 6 degrees of freedom
  - To measure the stability within the operating temperature range (33-260K) of all 4 quadrants with respect to the ORF in 6 degrees of freedom
- **Measurement Methods: limited to non-contact methods only**
  - We have developed test facilities to evaluate microshutter contrast and alignment stability at their 35K operating temperature. These facilities used a novel application of image registration algorithms to obtain non-contact, sub-micron measurements in cryogenic conditions.
- **Methods for X/Y/Z/Rx/Ry/Rz offsets, knowledge and stability**
  - Close range photogrammetry (ambient → cryo)
    - MSA high resolution cathetometer
    - Sub-pixel image analysis
- **Method for characterizing contrast of individual shutters**
  - Precise measurement of flux through open and closed shutters

$$Contrast = \frac{(OpenON - OpenOFF)/TimeOpen}{(ClosedON - ClosedOFF)/TimeClosed}$$

Example:

$$Contrast = \frac{(40{,}000 - 1{,}310)/2\,\text{sec}}{(1{,}600 - 1{,}310)/100\,\text{sec}} = \frac{19{,}345\,[\text{cts/sec}]}{2.9\,[\text{cts/sec}]} = 6{,}671$$

Opto-Mechanical Layout of '2D Photogrammetry' System

- **MSA evaluation facility: f/12 telescope simulator, cryostat and 1:1 imaging relay**
  - **Measures array contrast & alignment at ambient & cryogenic temperatures**
  - **Relates array displacements to ORF & measures stability over operating temperatures**
  - **Stages position both source and camera (same side as NIRSpec detector)**

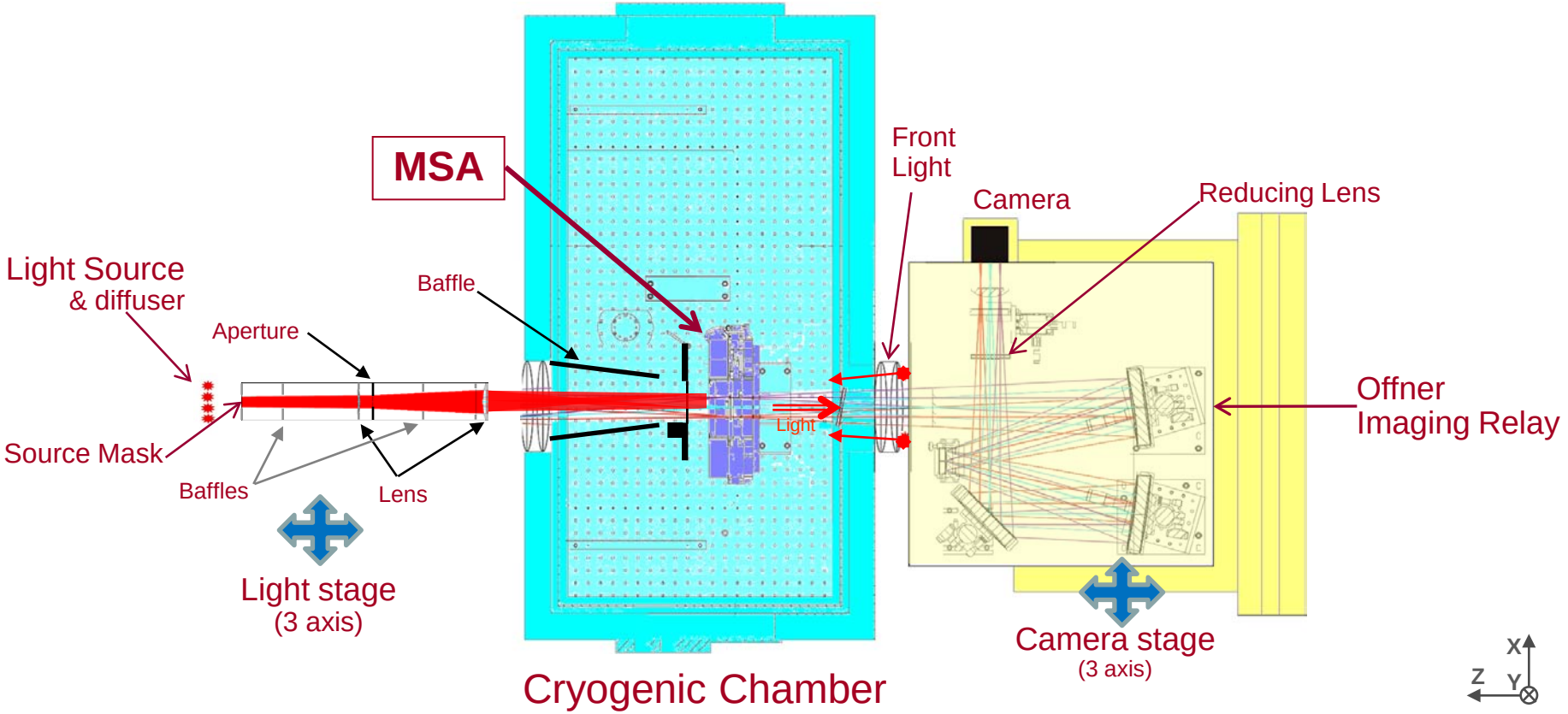

Test System Design – Equipment as built

MSA Evaluation Facility – GSFC Cryogenic Research & Integration Facility

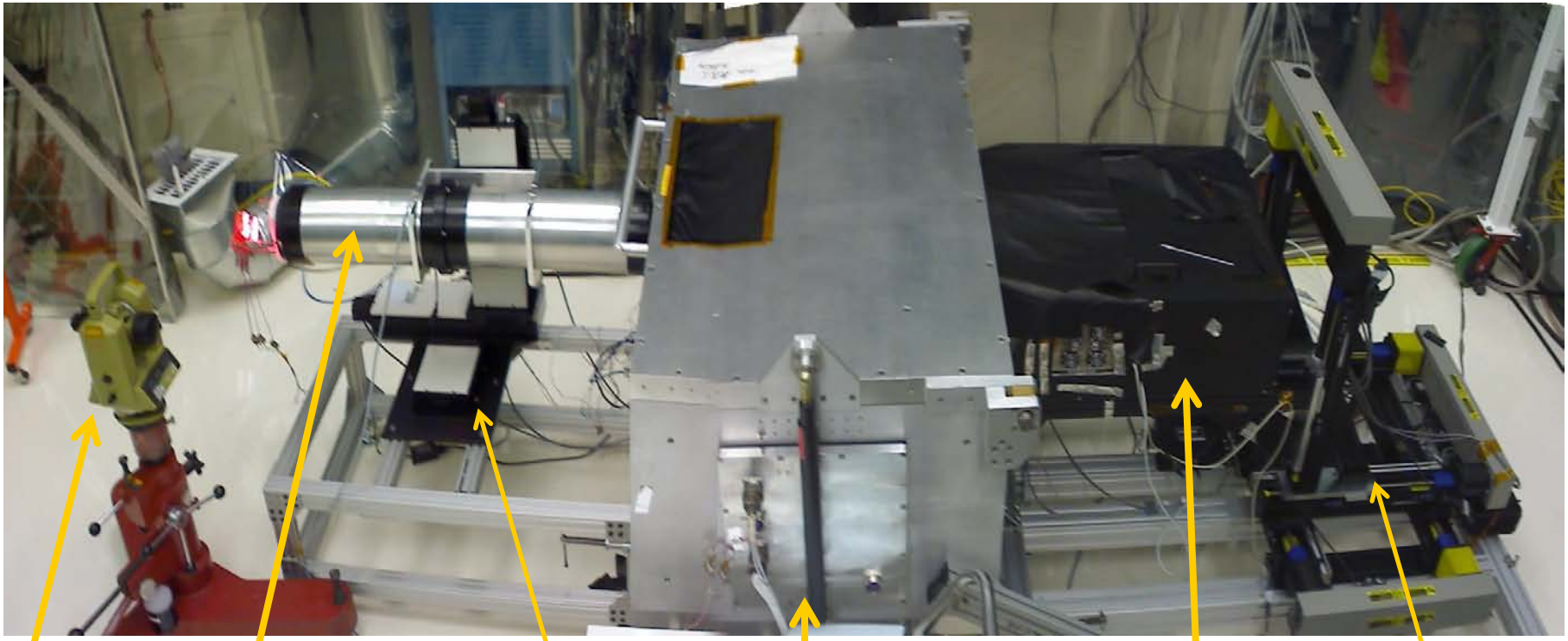

Test System Design – Components

- **Backlight Sources**
  - Red LEDs at 630nm
  - Incandescent bulbs with filters for IR
- **Backlight Stage** – positions source and mask to each of four quadrants
- **Reducing Lens** – 90% magnification allows camera to see entire quadrant at one time
- **Camera** – collects digital images for analysis
  - Cooled CCD detector for low noise
  - 16 Megapixel (4096 x 4096 pixels)
  - FOV (mm): 40.96x40.96, resolution: 9um/pixel

Backlight Stage

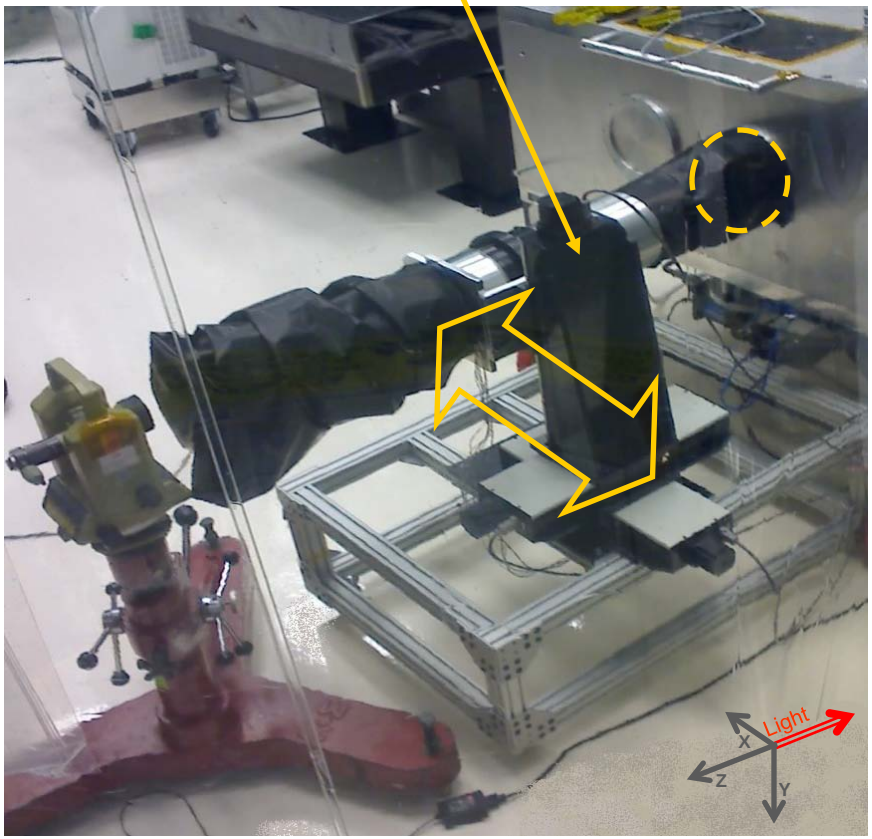

Focal plane of source

FM-MSA – Mosaic of Fully Open Images

- **Failed closed (dark areas) are shutters that did not open**
- **Failed opens are**
  - Shutters that did not close
  - Shutters with contrast below 500 (threshold), below 2000 (goal)

Location of Failed Opens (indicated with white circles)

Q1-52-102

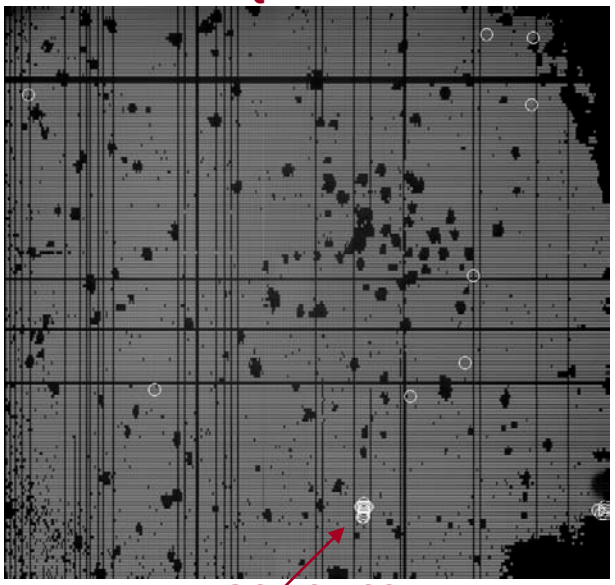

Q3-26-106

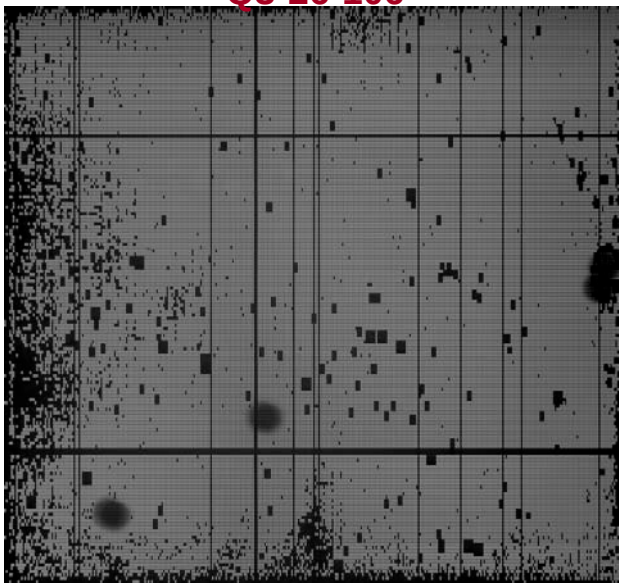

Q2-42-128

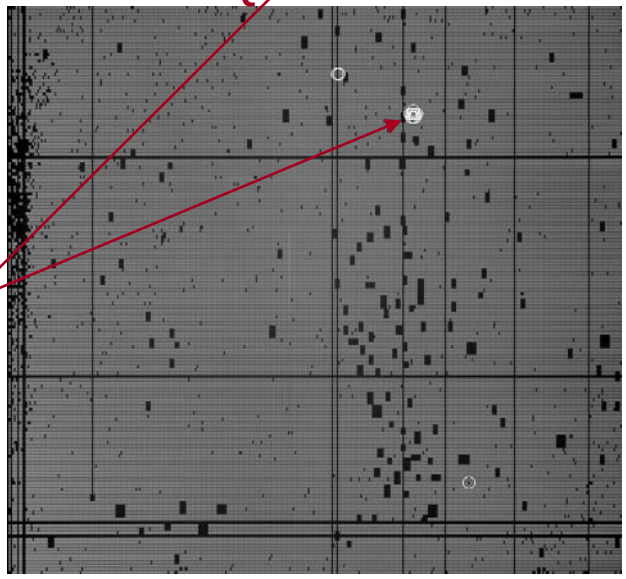

Q4-55-116

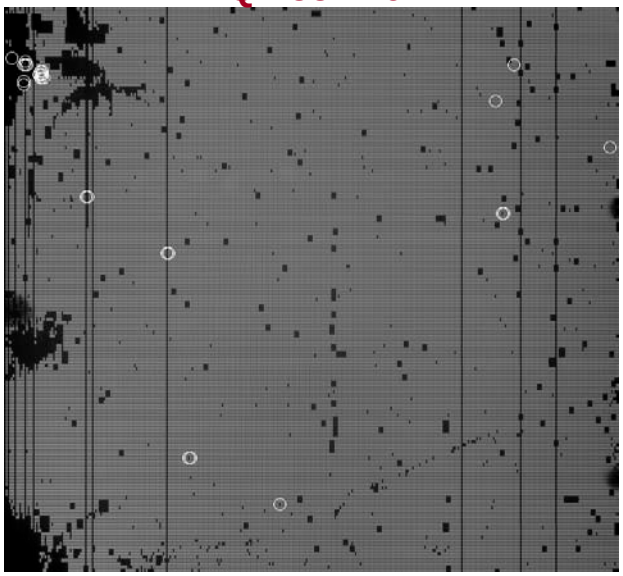

FM-MSA – Mosaic of Fully Closed Images

- **Failed opens (white spots) are**
  - Shutters that did not close
  - Shutters with contrast below 500 (threshold), below 2000 (goal)

Q1-52-102

Q3-26-106

Q2-42-128

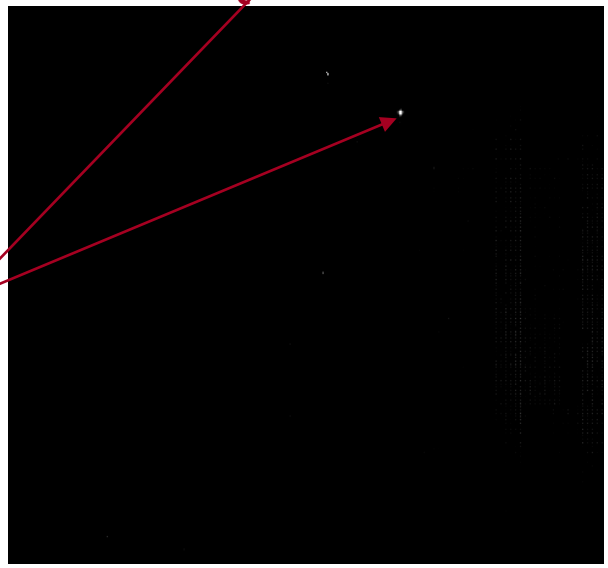

Location of Failed Opens

Q4-55-116

Systematic Error: Stray Light Influence on Contrast Measurement Capability

Mask at Light Source

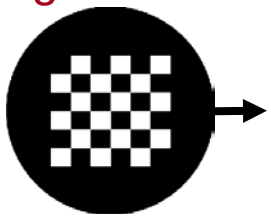

Image of closed array

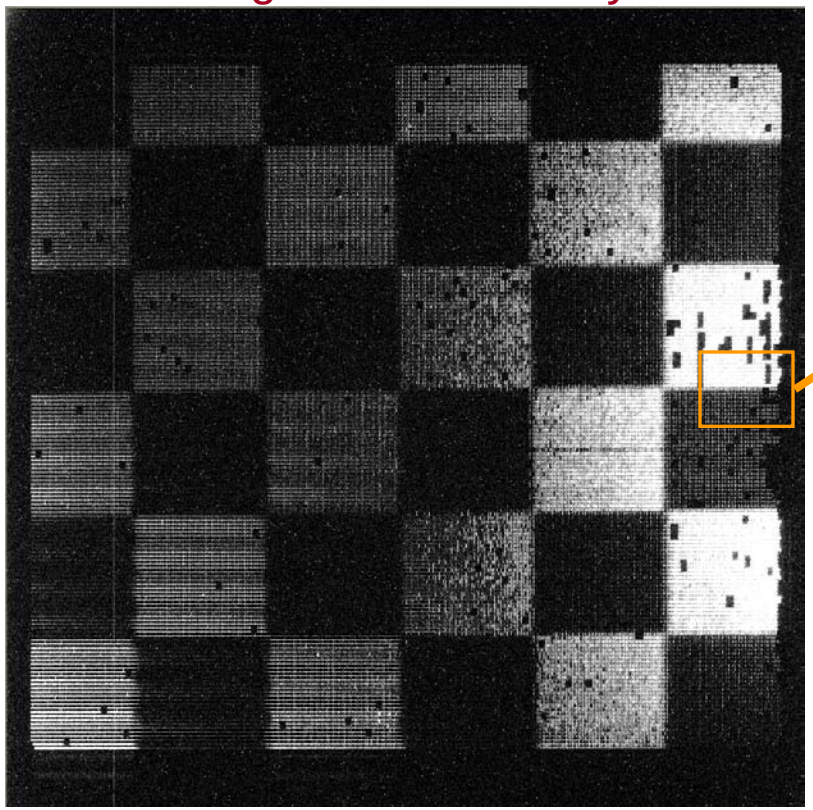

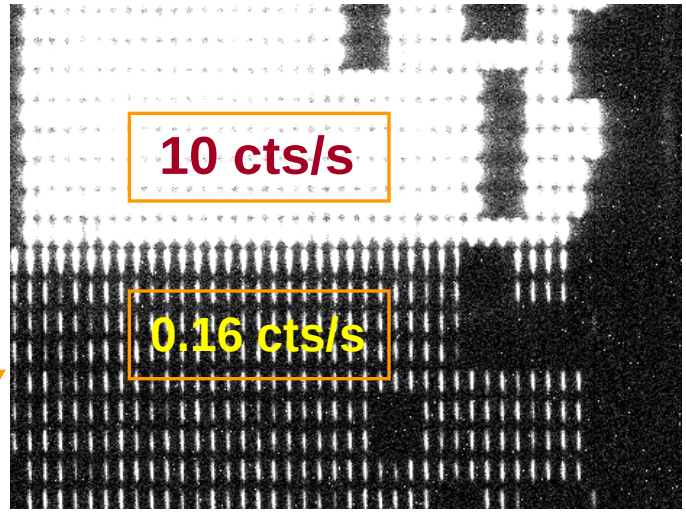

- ~1.6% light is from transmission through source mask
- Negligible stray light detected on back side
- No light on plugs in unlit area show NO scattered light on front side

- **Checkerboard source mask imaged through closed Q1 MSA position to determine extent of stray light in system with MSA installed**
- **No stray light effects detected**

MSA Level Visible (0.6 μm) Contrast

- Visible contrast maps of the four flight quadrants as they are viewed by the NIRSpec detector
- Each pixel in the image represents a single shutter's contrast value in grayscale
- Shutters below 2K contrast are color coded as per the side scale indicates
- To aid visibility of 'failed open' shutters, appropriately colored circles have been added around the failures.

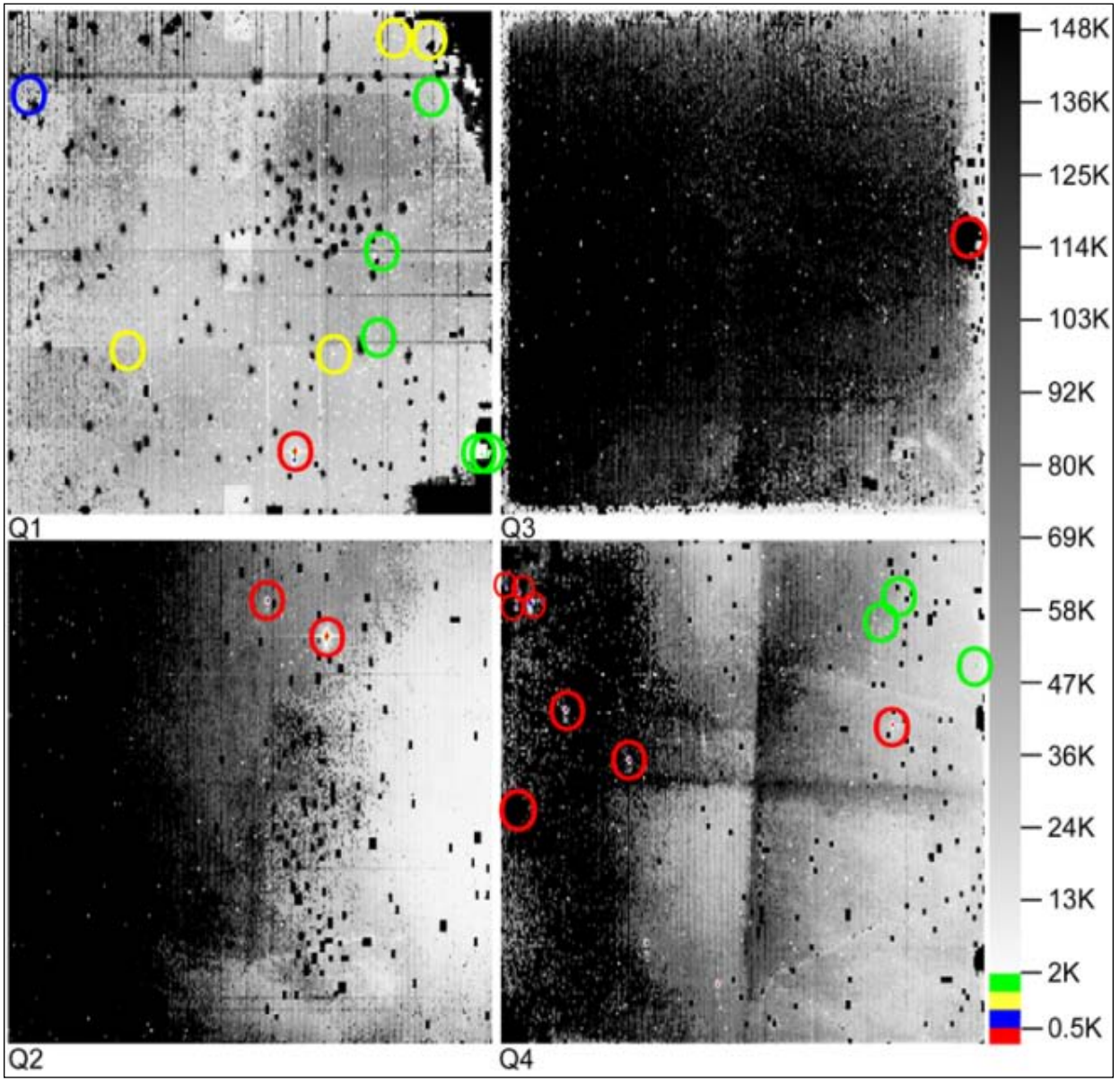

Quadrant Level 1.6 µm Contrast

- 1.6 µm contrast of flight shutters measured at quadrant level
- Each quadrant image acquired in 9 mosaic tiles and stretched to different grey scales
- Colored circles denote leaking areas not identified during visible contrast measurements
- Further comprehensive analysis completed to identify ‘unique’ IR failures

Q1-52-102: 1 Region: 13K

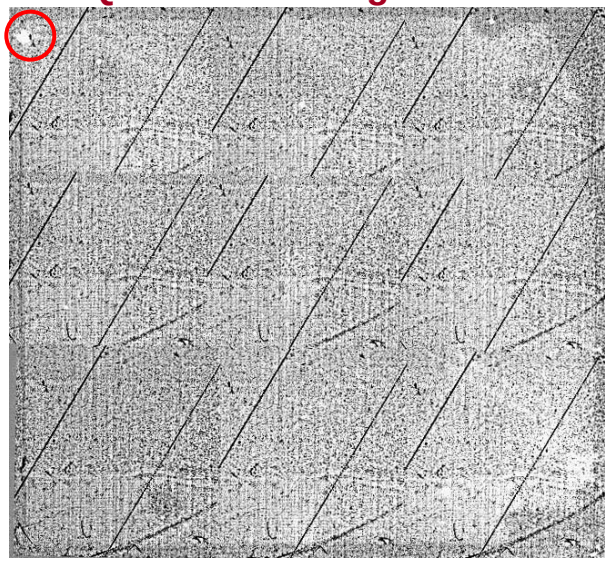

Q3-26-106: 3 Regions: 16K-17K

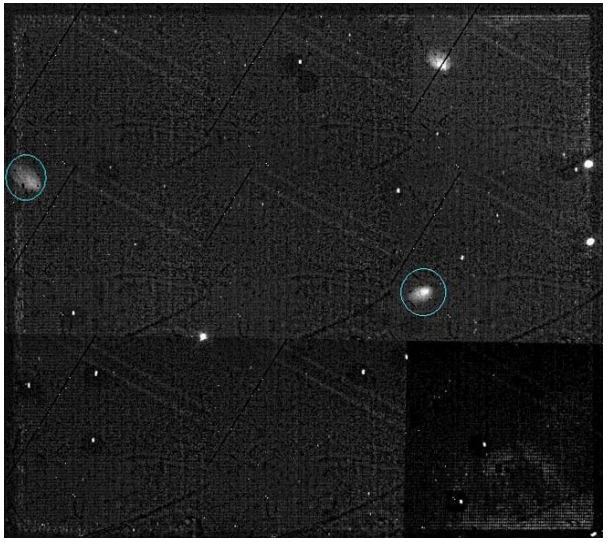

Q2-42-128: 9 Regions: 10K-13K

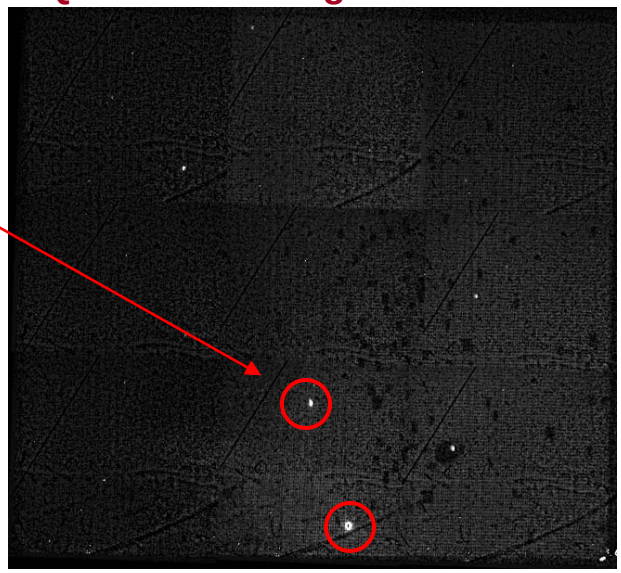

Q4-55-116: 1 Region: 8K

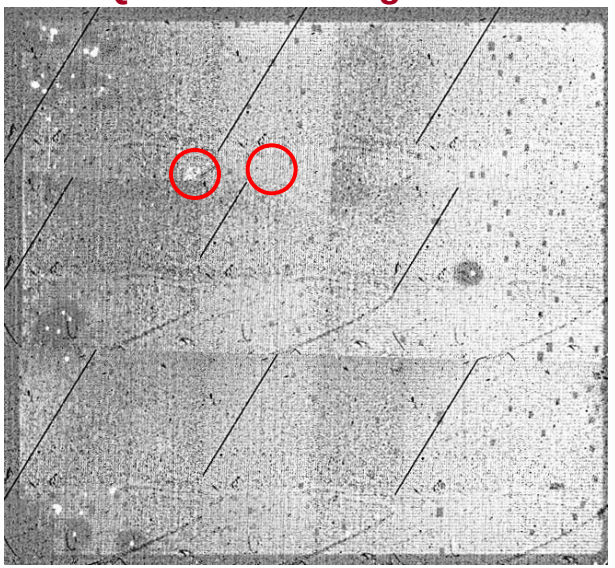

Summary of Mechanisms For Failure

Blue for Open Shutters. Black for Failed Closed Shutters. Orange & White for light leaks.

Light Shield Damage (4)
- Very Low Contrast (<500)
- Non-recoverable

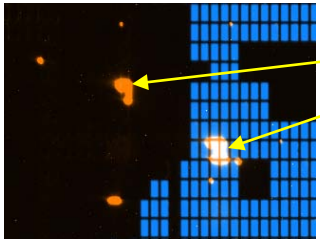

Wedged-Twisted (5)
- Very low Contrast (<500);
- Possible to release by warming

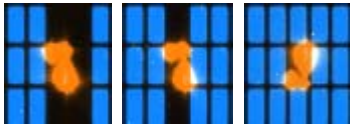

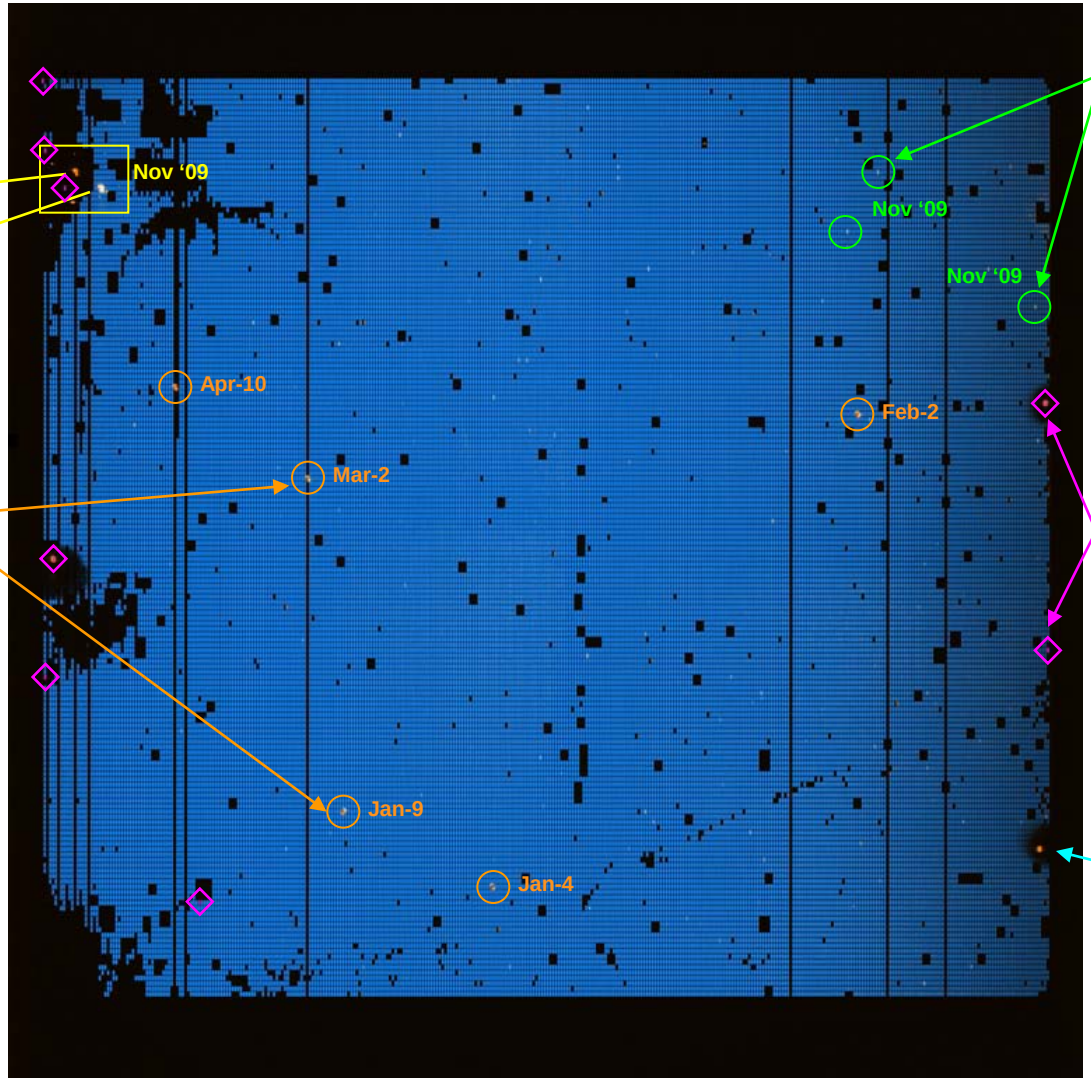

Mostly Closed Flat (3)
- Low Contrast failure (1000-2000)
- Possible to 'reset' by warming quad

Intermittent (3)
- Can be released by warming

Masked Shutters (1)
- A failure excluded by blocking light at light source, areas excluded until plugged and re-measured;

Summary of MSA Contrast Results

- Histogram displays visible contrast distribution of individual shutters
- Yellow line indicates 2K contrast requirement, green line denotes 100K contrast goal
- Results indicate performance is acceptable for observation goals

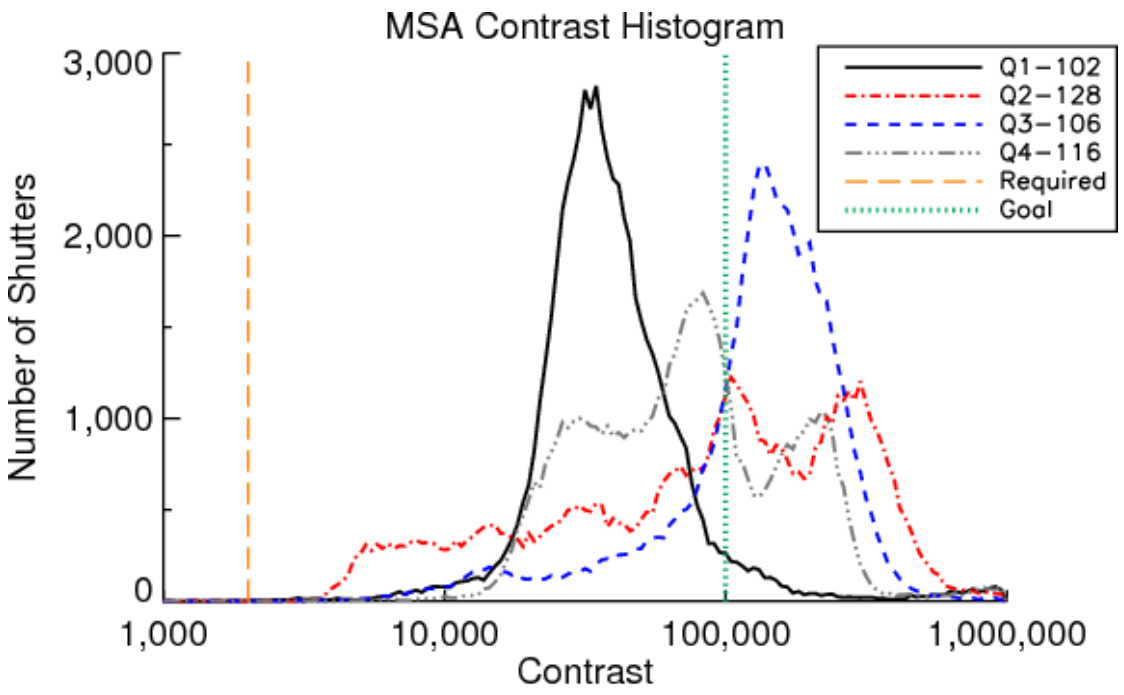

Quad ID	Q1-52-102	Q2-42-128	Q3-26-106	Q4-55-116
Total F/O	27	3	6	21
Total F/C	9,531	5,997	12,087	5,601
Avg. Visible Contrast	38,500	78,000	120,000	71,000
H Band IR	13,400	13,000	16,600	7,600

All Values in blue are from B11 Quadrant Test Facility

Shutter Alignment: Photogrammetric Sub-pixel Image Analysis

- **Hardware additions providing well-focused targets for photogrammetrical image analysis**
  - Retardation Plates for Ambient to Cryo offset
  - Minilens array for X-Y Stability: improve image sampling from 9um/pixel to 3µm/pixel
- **Two image analysis methods to determine location of arrays WRT ORF in images**
  - Front-lit alignment of all arrays at Ambient & Cryo
  - Cruciform surface and corners of four quads seen in each image
  - Red, green and blue boxes indicate regions selected for image registration analysis
- **National Instruments (NI) Vision algorithm - standard pattern-matching function performing a normalized cross-correlation method**
  - Analysis of motion in the Z and RZ directions through stability cycles and analysis of cryogenic offset images
  - Measured offsets to $^1/_{3^{rd}}$ pixel → 4 µm
- **Unser Registration Method - wavelet decomposition of 2D images into low-to-high frequencies, similar to Fourier transforms**
  - Limited to analysis of X & Y motion during 30K stability cycles due to requiring stable shutter fields
  - Measured Stability to $^1/_{10^{th}}$ pixel → 1 µm

Swappable Retardation Plates Fixture Enabling Simultaneous Focus

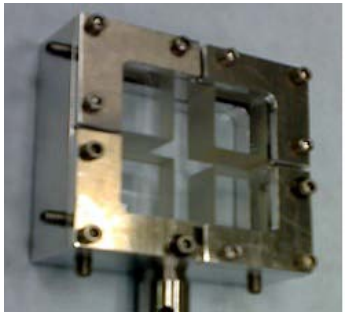

Offsets: Field of View Through Plate Fixture

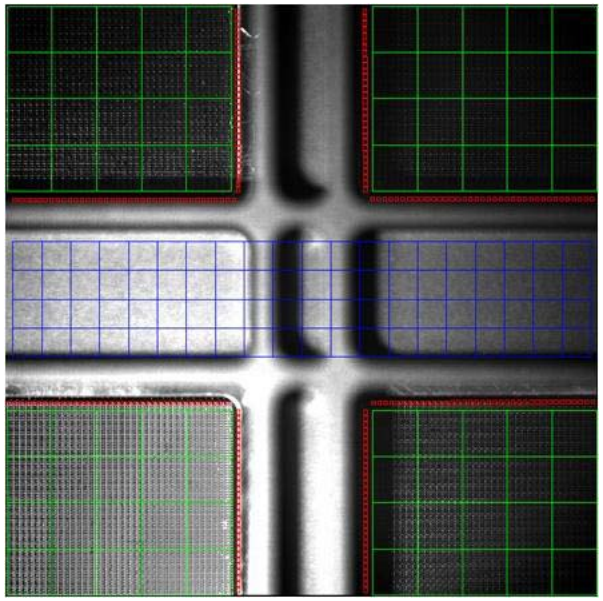

Swappable Array of Mini Lenses Producing 3X Magnification

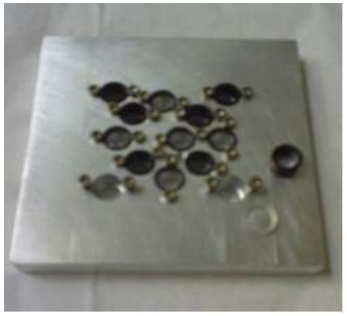

Stability: Field of View Through Mini Lenses

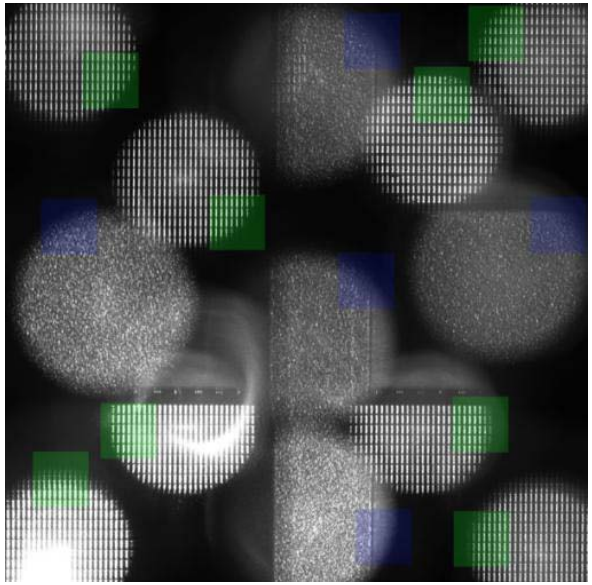

Cool-Down Offsets Temperature Profile

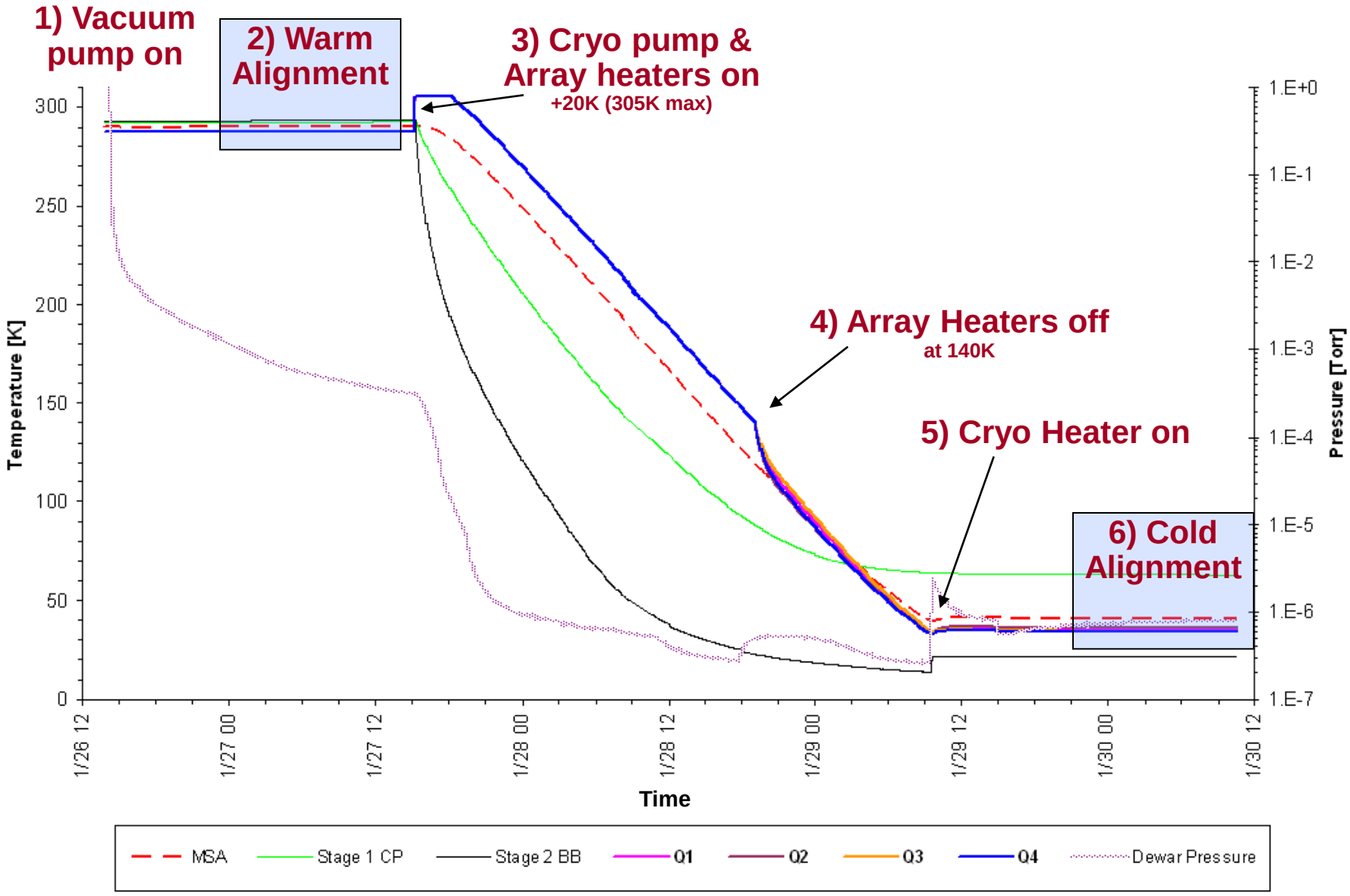

Alignment Repeatability for Multiple Cooldowns – Offsets in X,Y,Z

- Meets Req for Alignment Offset (± 100 microns)
- Arrows ( ) indicate direction of quadrant motion
- Y measurements greater due to snubber deflection

Alignment Offsets [microns]

	X	Y	Z
Q1	8	26	7
Q2	5	-45	-14
Q3	-6	20	21
Q4	-3	-36	-11
Offset Req.	±100	±100	±100
Knowledge	±5	±15	±25
Knowl. Req.	±5	±5	±5

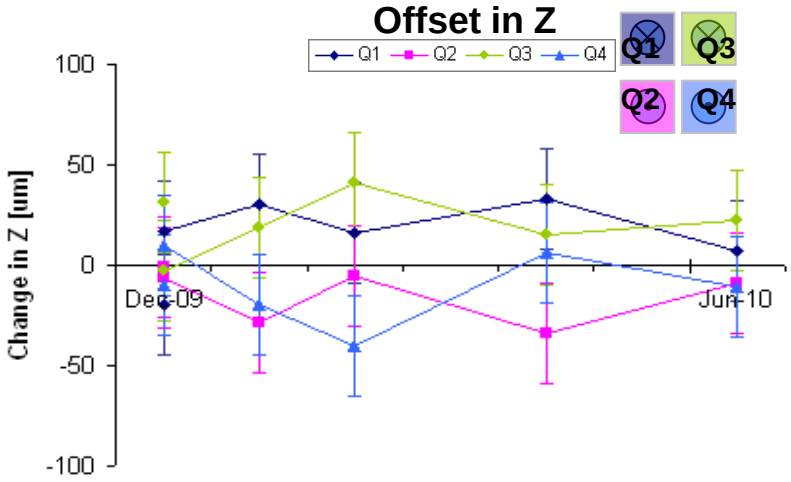

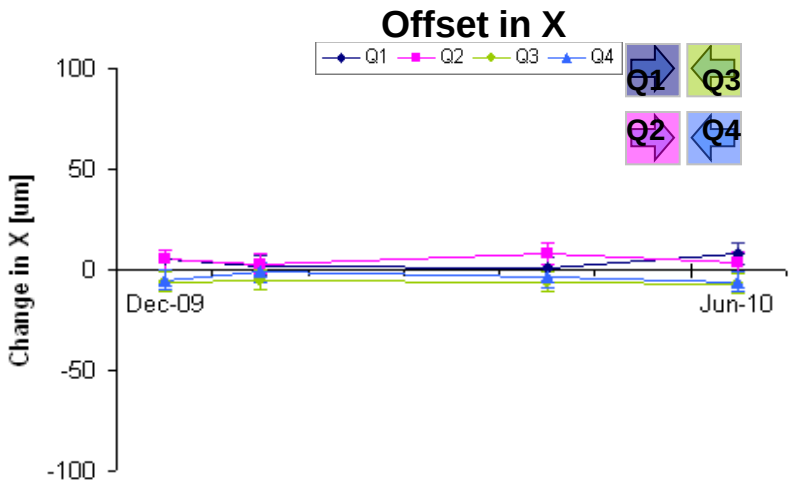

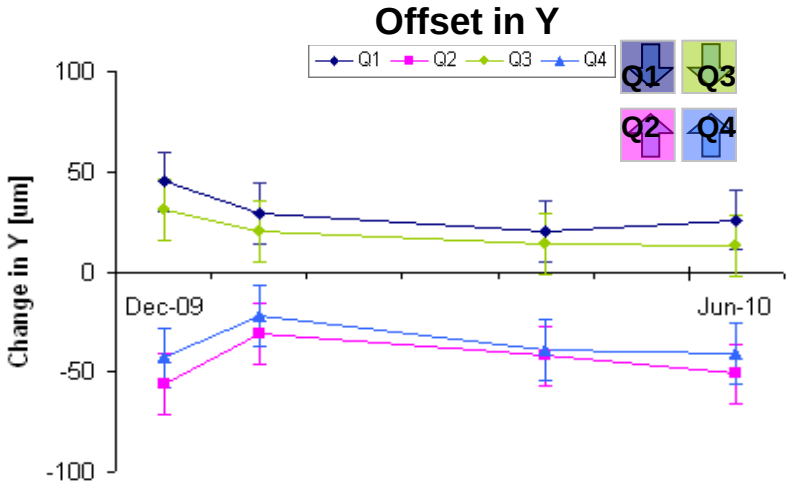

* Average position (i.e. average of locations measured on each Quad): X=8.9mm, Y=10.2mm from ORF center

Alignment Repeatability for Multiple Cooldowns – Rotations around X,Y,Z dir.

- **Meets Req for Alignment Rotation (± 500 micro-radians)**

Alignment Rotations [microradians]

	X	Y	Z
Q1	-44	29	443
Q2	6	20	-355
Q3	-2	-10	-219
Q4	32	-34	414
Offset Req.	±500	±500	±500
Knowledge	±110	±110	±100
Knowl. Req.	±50	±50	±50

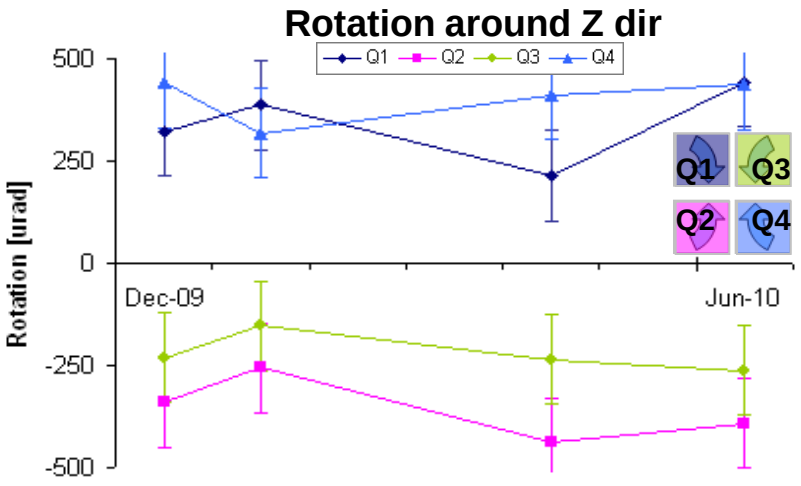

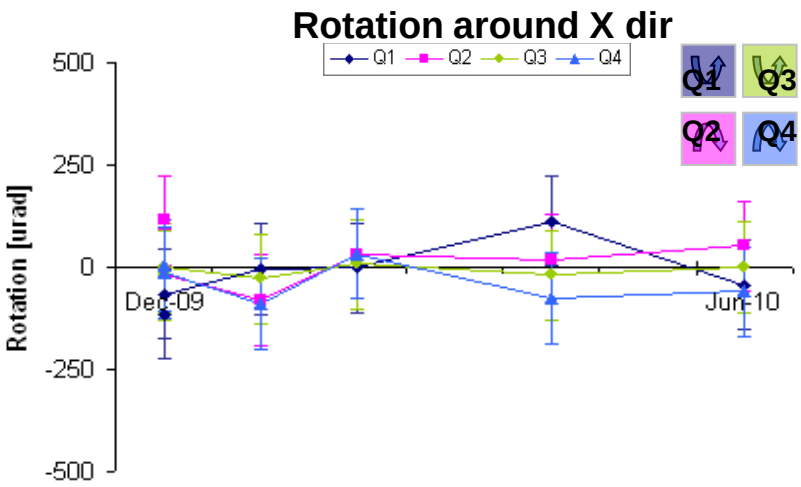

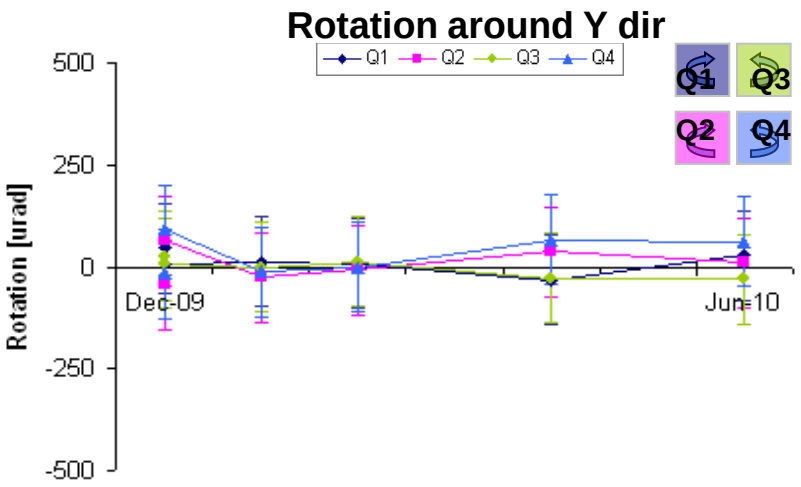

* Average position (i.e. average of locations measured on each Quad): X=8.9mm, Y=10.2mm from ORF center

Alignment Stability Temperature Profile

Four 'Shutter Release' Heat Cycles to 260K

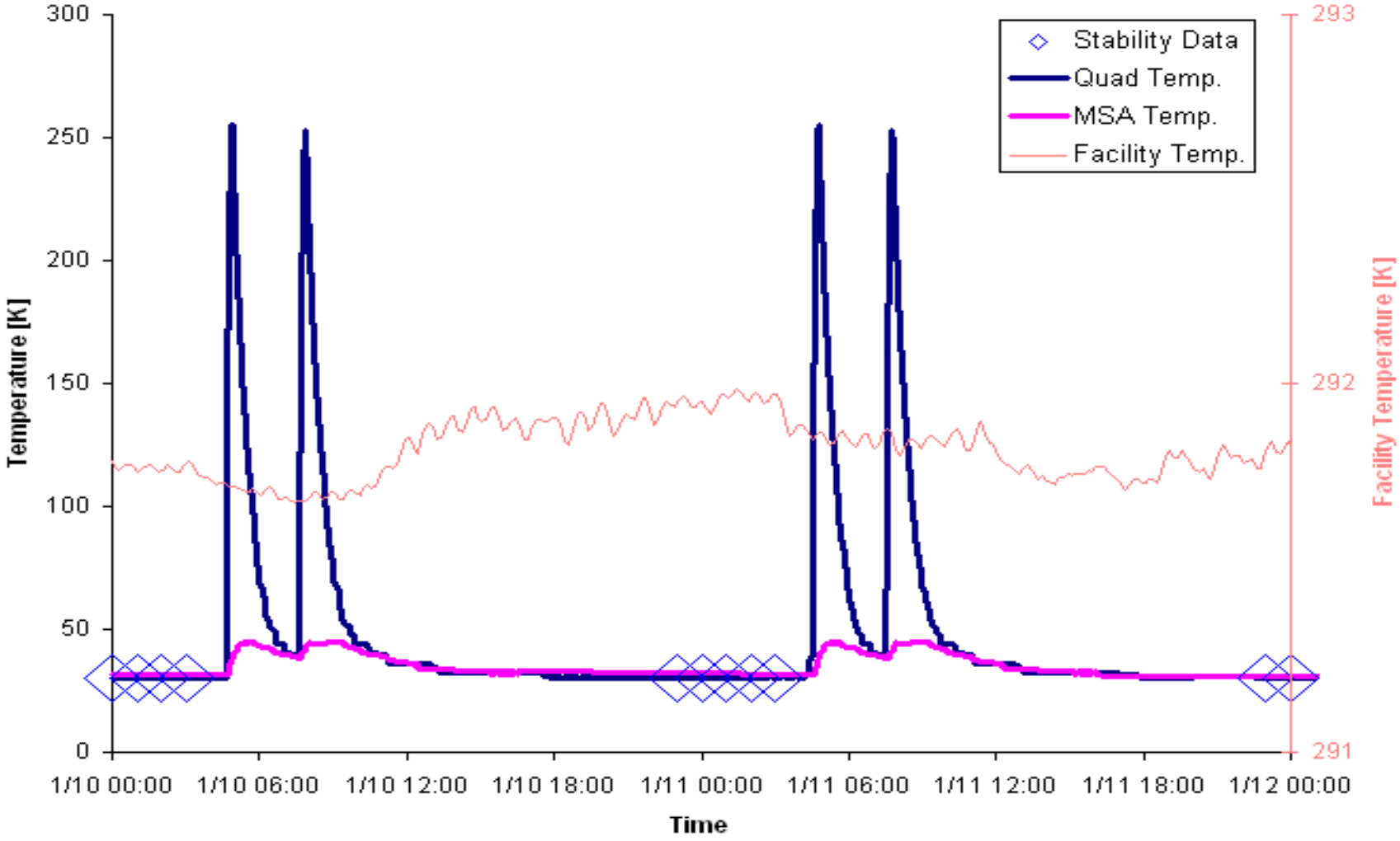

Quadrant Stability In & About the X, Y & Z Axes

Four 'Shutter Release' Heat Cycles to 260K

- Performed 2 consecutive stability cycles
- Offset in X,Y & Z was measured before and after each cycle
- Rotational offsets measured about Z only
- Alignment Stability is passing Requirements

Stability Results (Zero-To-Peak)

Stability of	Q1	Q2	Q3	Q4	Req
Offset in X [μm]	0.2	0.2	0.2	0.2	1
Offset in Y [μm]	0.5	0.3	0.7	0.3	1
Offset in X-Y plane [μm]	**0.5**	**0.3**	**0.7**	**0.3**	1
Offset in Z [μm][e]	**8**	**6**	**5**	**1**	10
Rotation around Z [rad][e]	**8E-6**	**1E-5**	**1E-5**	**1E-5**	1E-5
Rotation around X or Y [rad]	***NA*[ETU]**				5E-5

e Start to finish comparison (before 1st cycle to after last cycle)

ETU ETU test results; not feasible on flight hardware

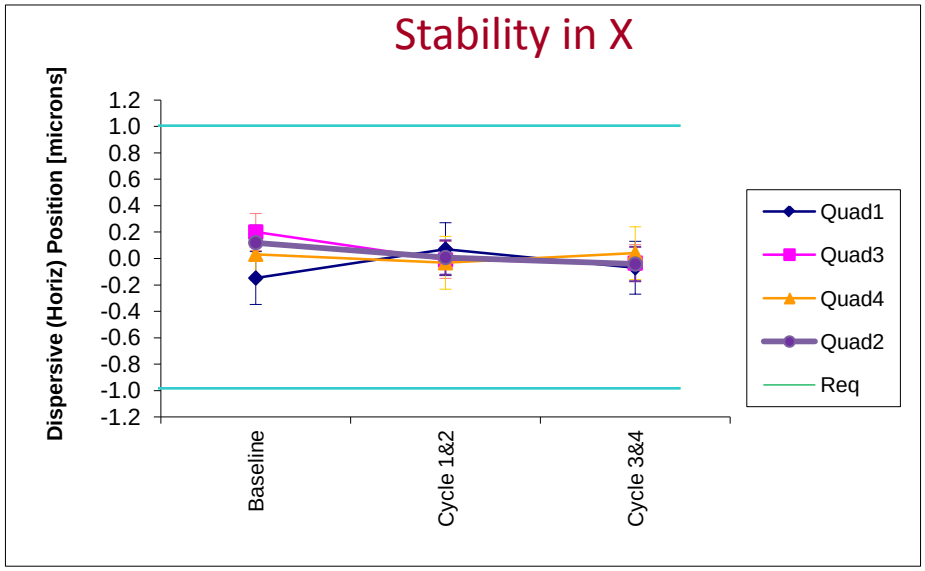

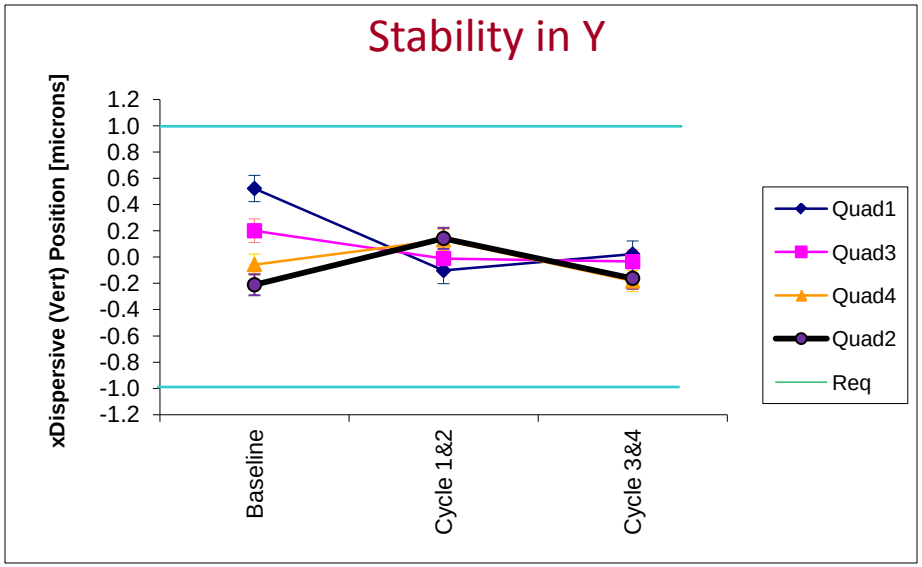

MSA Optical Metrology Conclusions

- Our test program has demonstrated that the MSA assembly includes focal-plane object selectors that are both high contrast and cryogenically stable.
- By direct measurement, we find that the Open-Closed contrast of the MSA shutters are greater than 2000 in the 0.6 to 5 μm wavelength range and that the percentages of failed closed and failed open shutters are acceptably low to fulfill mission requirements.
- Results of characterizing the cryogenic motion of the shutters show that microshutters are stable to within 0.5μm and contract from ambient position in a predictable and repeatable manner.
- Stable and predictable shutter positions will ensure that spectra acquired by NIRSpec will be accurate. Long-term shutter stability across periodic heat cycles will ensure costly time is not lost in repeating spectrograph calibrations.
- The MSA level of performance confirms that the NIRSpec instrument will be adequately efficient to meet JWST's goal of observing 2500 galaxies in five years.

Test System Images

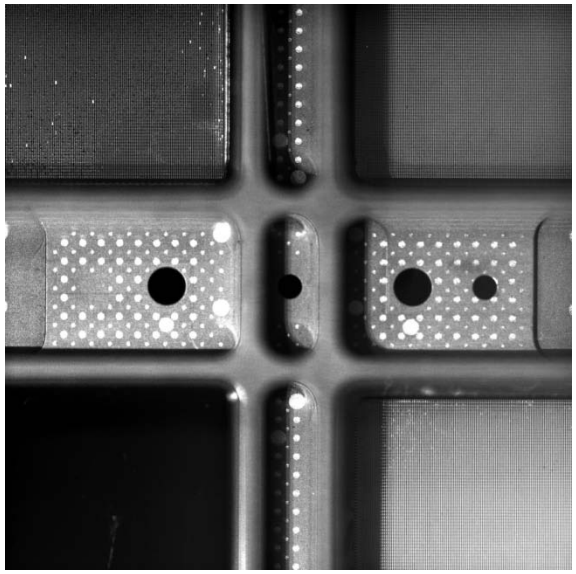
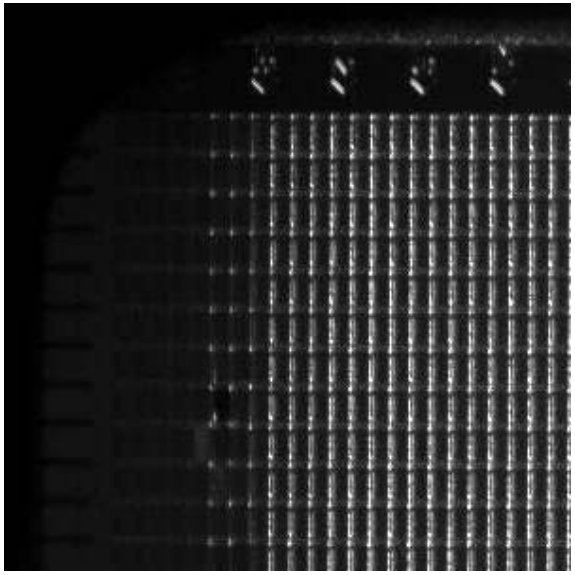
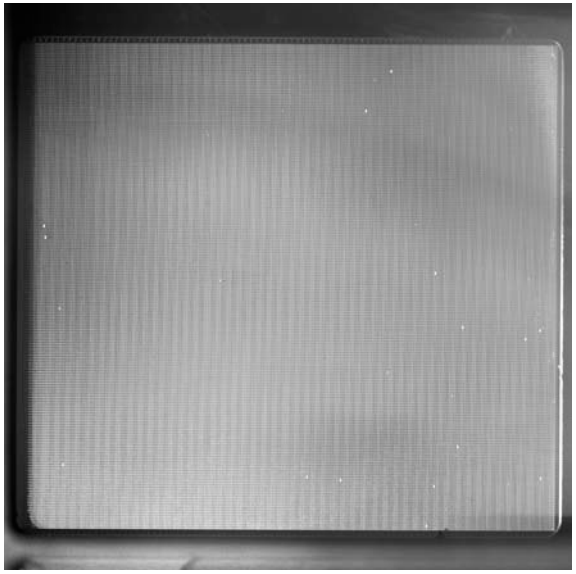
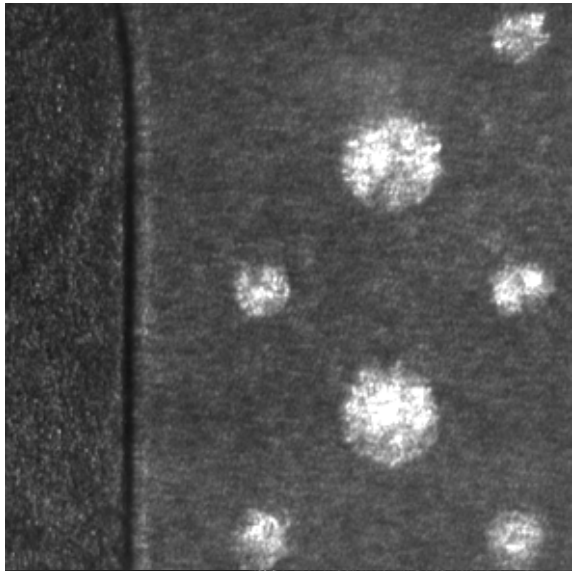
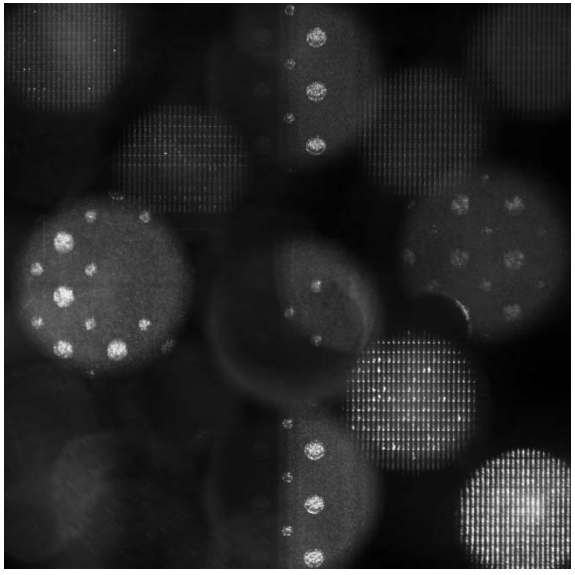


ADDITIONAL SLIDES

ETU Quad Stability in X,Y,Z: 20 cycles

Quadrant stability shows no trend over 20 cycles
ETU results show no 'creep' in position of quadrants w.r.t ORF over multiple cycles

Worst Case Quad Results, Zero-To-Peak

	7 Hours	13 Hours	Req.
Stability in X [um]	1.2	0.4	±1[W1]
Stability in Y [um]	0.8	0.6	±1[W1]
Stability in Z [rad]	NA	-10	±10

[W1] **Requirement waiver to 1.0 microns from 0.4 microns.**

Stability in Z

	Q1	Q3	Q4	Req.
Pretest Z [um]	-6	-19	27	--
Posttest Z [um]	-4	-9	26	--
Change in Z [um]	-2	-10	-1	±10

Stability in X

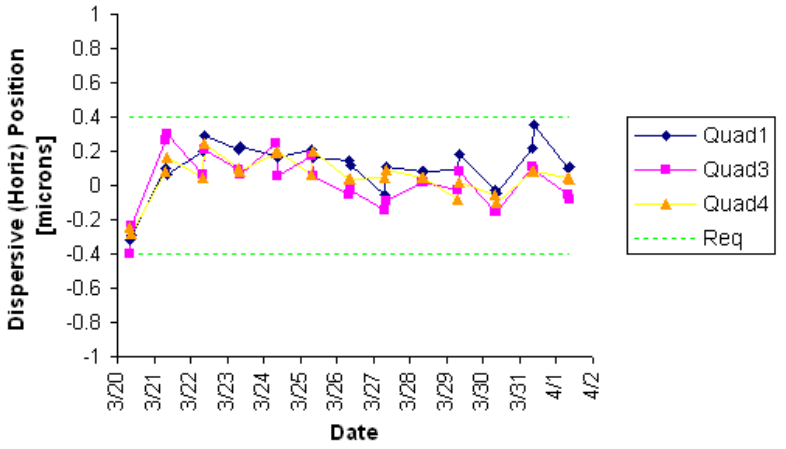

Stability in Y

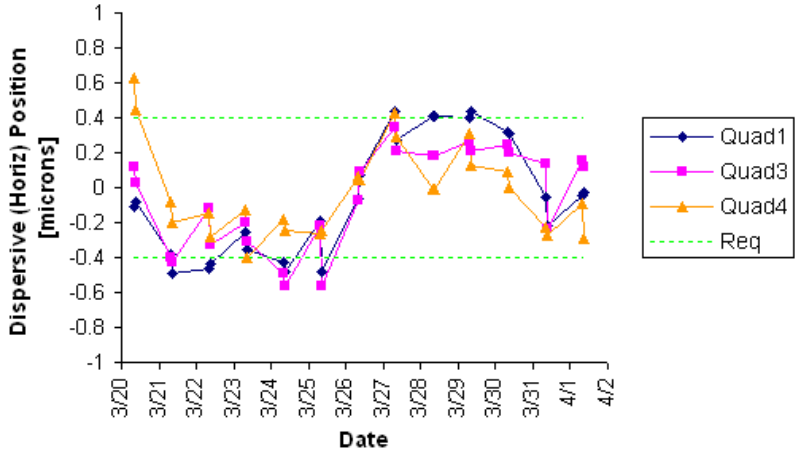

Rationale for Limiting Infrared Contrast Measurements to H-Band

- Contrast of ‘Non-Flight’ Array 107 measured at visible, 1.6 µm ‘H-band’ and 2.2 ‘K-band’
- Array 107 measurements show lowest contrast at 1.6 µm from light passing through shutter support structure
- Results show higher frequencies blocked by silicon substrate, lower frequencies diffracted at high angles
- Based on 107 results, contrast of flight quadrants, MSA structure measured at visible and 1.6 µm ‘H-band’ only
- Visible and H-band contrast results of flight quadrants and structure are above acceptance levels

Limiting Infrared Contrast Measurements to H-Band (3/3)

IR-Leak Mechanism: Support structure transmission dominating shutter latching performance

- **Gaps to avoid electrical shorts allow scattering through silicon structure**
- **Gaps 'glow' uniformly when illuminated**
- **IR contrast less dependant on measurement position**

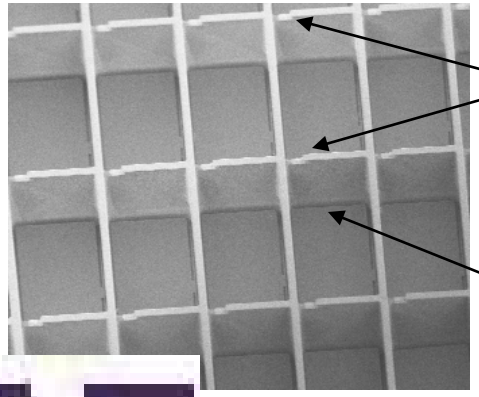

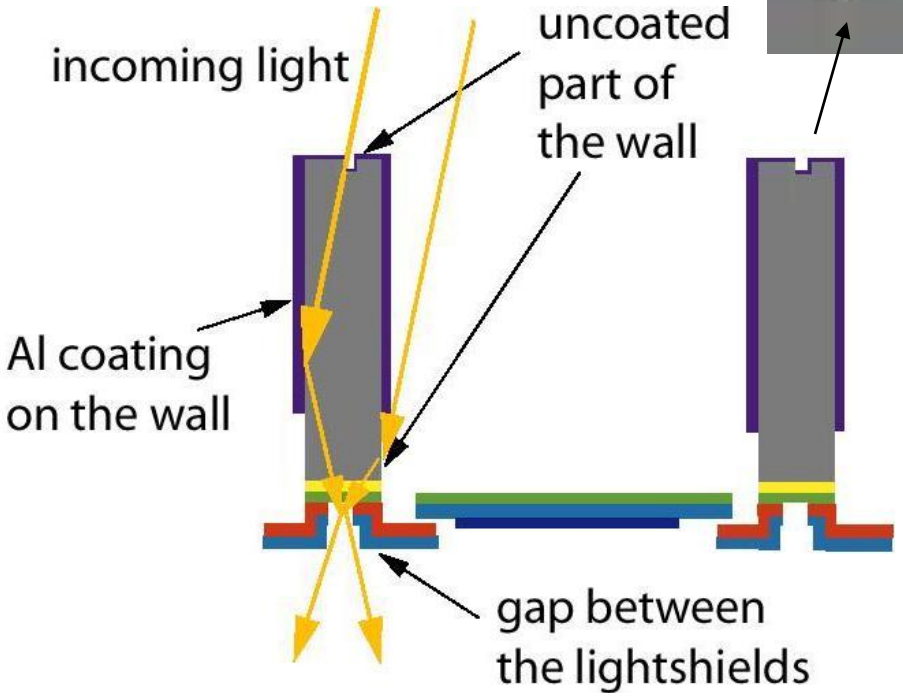

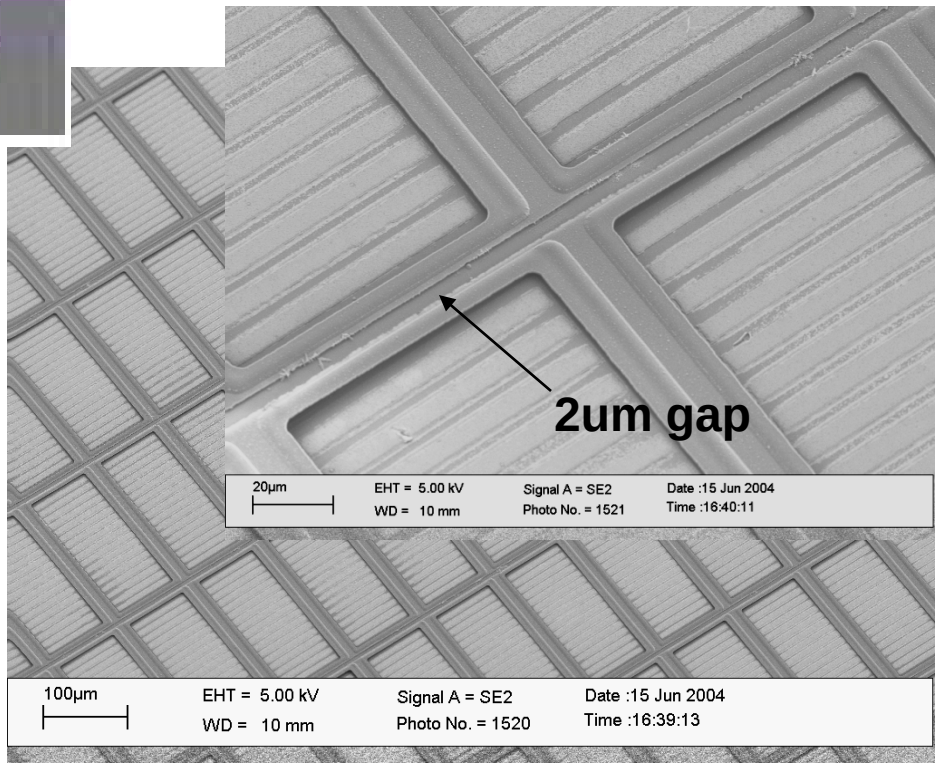

Review of System Error

- **Statistical errors (not limited)**
  - Post processing of images
  - Signal photon noise & dark current
  - Camera read noise
- **Systematic errors (limited)**
  - Camera non-linearity (below 2%)
  - Camera persistence
  - Illumination non-uniformity
  - Scattered light around MSA structure
  - Scattered light and ghosting after array [2-10% at low contrast values (2K), and array contrast distribution dependent]

Note: F/10 beam provides conservative estimate of contrast

Systematic Error: Camera Linearity

- Linearity measured with constant illumination
- Average counts measured against varied exposure time
- Data points follow linear trend line
- Error from linearity negligible

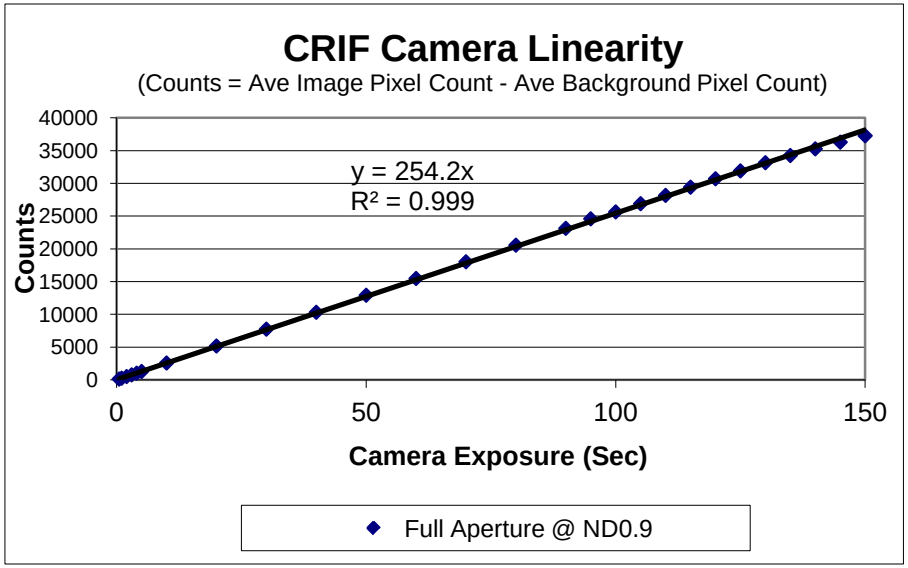

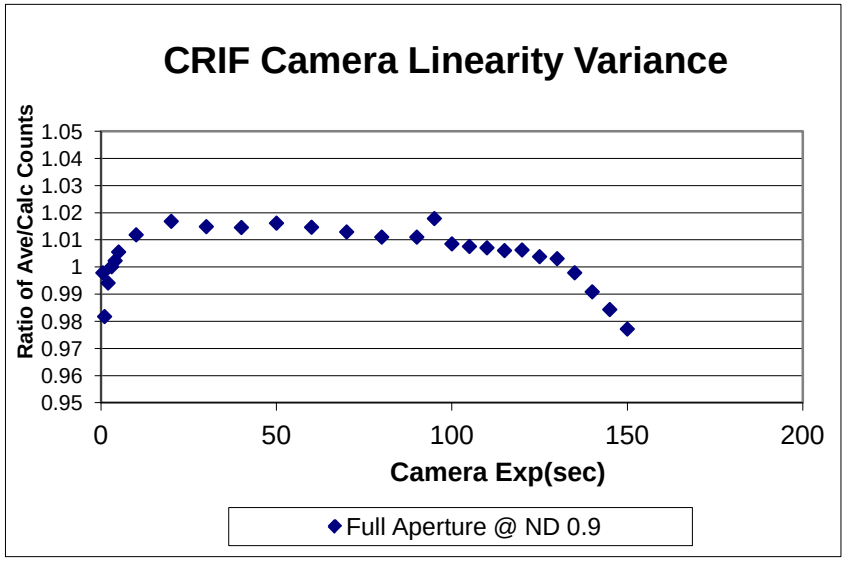

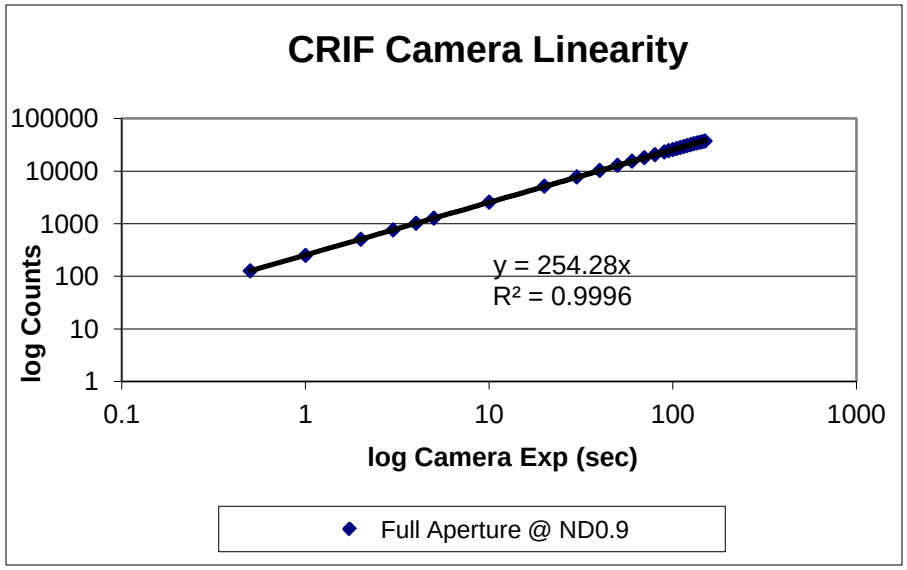

Systematic Error: Stray Light Influence on Contrast Measurement Capability in the Visible

- Pinhole array used to simulate failed opens, source mask aligned over ‘failures’
- Mask attenuation of failed opens by 71.4x
- Stray light ghost analysis compared to failed open: Bright Ghosts = 2x10-3, Dim Ghosts = 2x10-4, ghosts dimmed to 6x10-5 with source mask allowing up to 10K contrast measurement
- Maximum contrast capability: 49K near failed opens (worst case/red annuli), 56K away from failed opens (best case / blue regions), exceeding 2K spec

Source Mask

20 Second Exposure w/o Mask

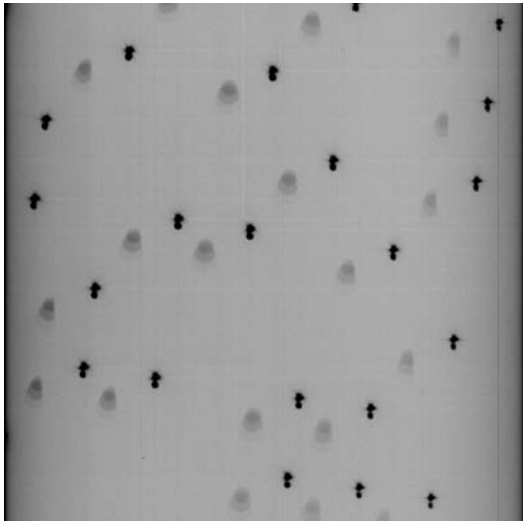

1000 Second Exposure w/ Mask

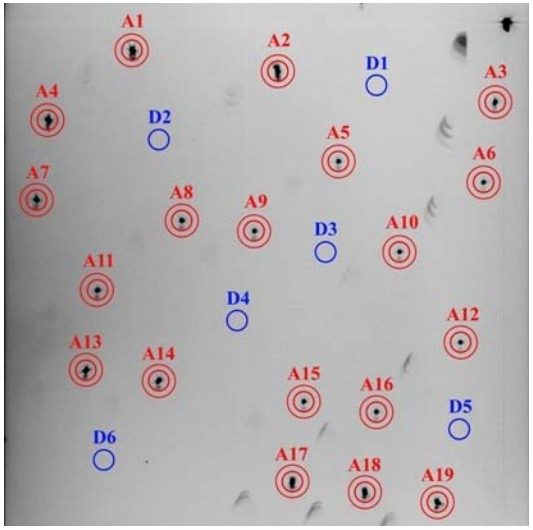

	Near failed opens	Away from failed opens
Contrast	**49,000**	**56,000**

Contrast capability exceeds 2,000 Requirement

Contrast Measurements Highly Repeatable

Contrast *Operating Shutters Only	Non-Flight Q1-37-137			Q3-26-106		
	Apr 9 pm	Apr 10 am	Delta	Apr 12 am	Apr 12 pm	Delta
Average	22,512 $10^{4.35}$	23,295 $10^{4.37}$	3%	121,558 $10^{5.15}$	120,821 $10^{5.08}$	1%
Std. Dev, σ	16%	16%	0	5%	5%	0
# shutters <2000	7,919	7,931	0.2%	0	0	0
# shutters <500	483	422	13%	0	0	0
Prior Magnet cycles[a]	38	42	(4)	48	57	(9)

[a] Since last time at ambient

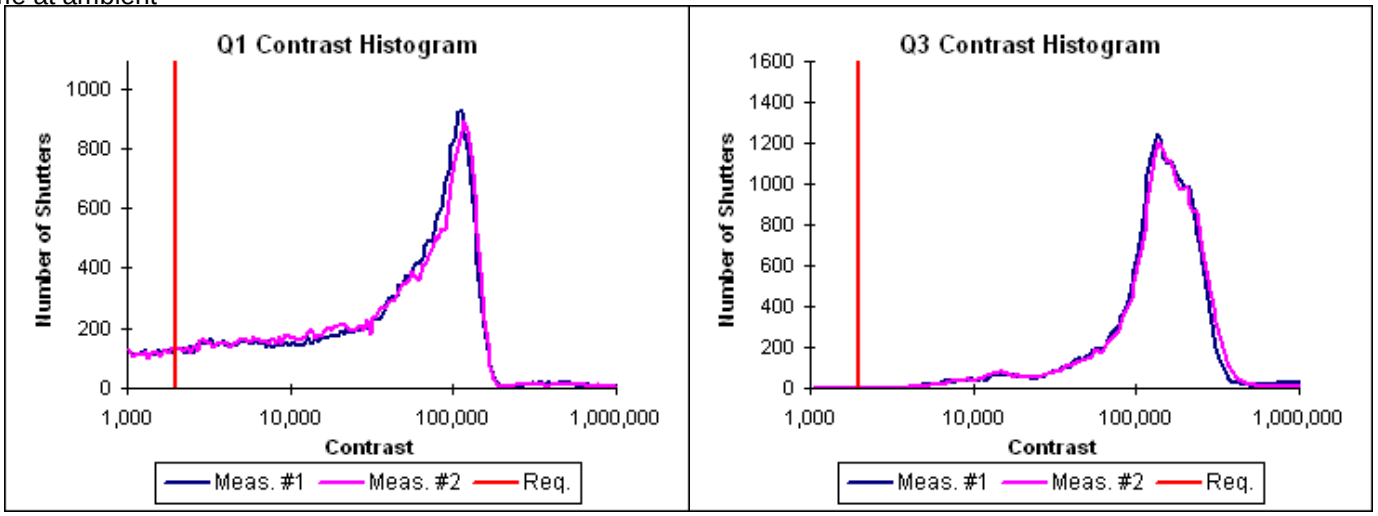

Contour Maps of MSA Level Contrast

Q1-52-102

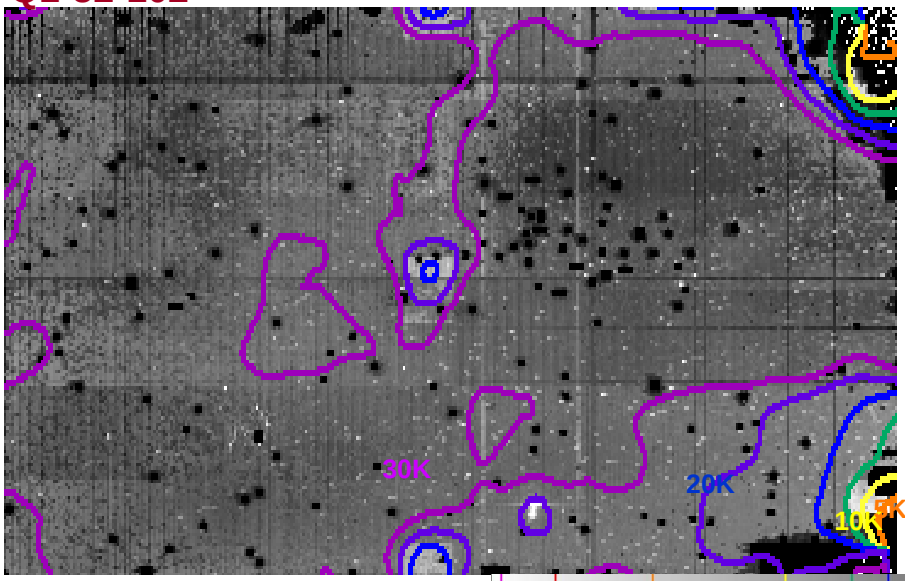

Q3-26-106

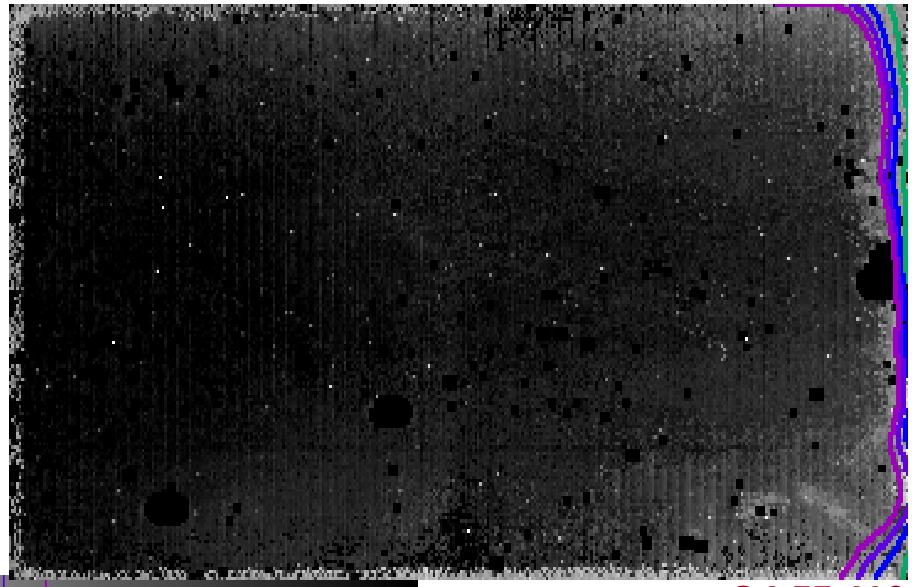

Q2-42-128

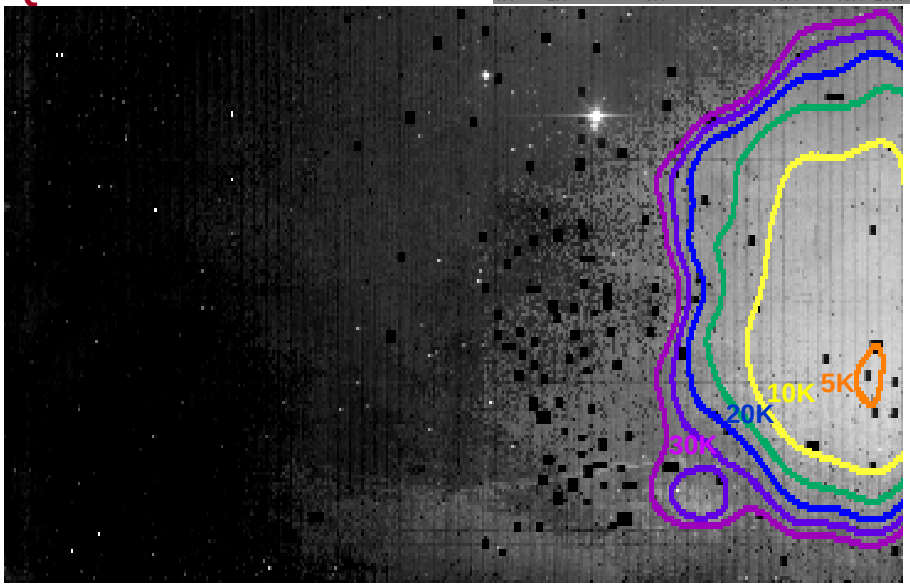

Q4-55-116

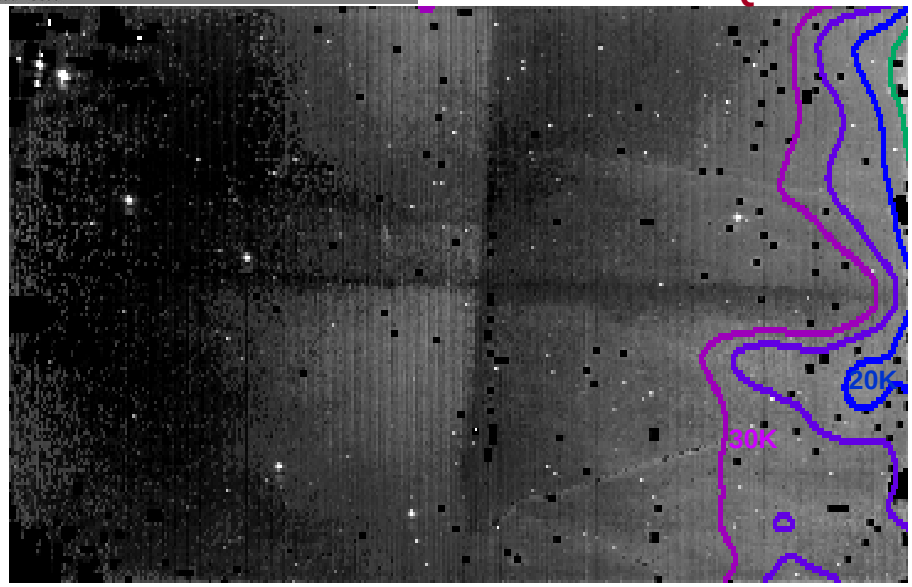

Plugging Failed Open Shutters

Plugging Failed Open Shutters